



HAL
open science

Neuroanatomy and pneumaticity of the extinct Malagasy “horned” crocodile *Voay robustus* and its implications for crocodylid phylogeny and palaeoecology

Gwendal Perrichon, Yohan Pochat-cottilloux, Davide Conedera, Pascale Richardin, Vincent Fernandez, Lionel Hautier, Jeremy E Martin

► To cite this version:

Gwendal Perrichon, Yohan Pochat-cottilloux, Davide Conedera, Pascale Richardin, Vincent Fernandez, et al.. Neuroanatomy and pneumaticity of the extinct Malagasy “horned” crocodile *Voay robustus* and its implications for crocodylid phylogeny and palaeoecology. *The Anatomical Record: Advances in Integrative Anatomy and Evolutionary Biology*, 2023, 10.1002/ar.25367 . hal-04357702

HAL Id: hal-04357702

<https://hal.science/hal-04357702>

Submitted on 21 Dec 2023

HAL is a multi-disciplinary open access archive for the deposit and dissemination of scientific research documents, whether they are published or not. The documents may come from teaching and research institutions in France or abroad, or from public or private research centers.

L'archive ouverte pluridisciplinaire **HAL**, est destinée au dépôt et à la diffusion de documents scientifiques de niveau recherche, publiés ou non, émanant des établissements d'enseignement et de recherche français ou étrangers, des laboratoires publics ou privés.



Distributed under a Creative Commons Attribution 4.0 International License

RESEARCH ARTICLE

Neuroanatomy and pneumaticity of the extinct Malagasy “horned” crocodile *Voay robustus* and its implications for crocodylid phylogeny and palaeoecology

Gwendal Perrichon¹  | Yohan Pochat-Cottilloux¹  | Davide Conedera¹ |
 Pascale Richardin^{2,3}  | Vincent Fernandez^{4,5}  | Lionel Hautier^{6,7}  |
 Jeremy E. Martin¹ 

¹CNRS UMR 5276, Université Claude Bernard Lyon 1, ENS de Lyon, Laboratoire de Géologie de Lyon-Terre, Planètes, Environnement, Villeurbanne, France

²Centre de Recherche et de Restauration des Musées de France (C2RMF), Palais du Louvre, Porte des Lions, Paris, France

³CNRS-UMR 8068, Technologie Ethnologie des Mondes Préhistoriques (TEMPS), Université Paris Nanterre, Nanterre Cedex, France

⁴Imaging and Analysis Centre, The Natural History Museum, London, UK

⁵European Synchrotron Radiation Facility, Grenoble, France

⁶Institut des Sciences de l'Évolution, Université Montpellier, CNRS, IRD, EPHE, Montpellier, France

⁷Mammal Section, Life Sciences, Vertebrate Division, The Natural History Museum, London, UK

Correspondence

Gwendal Perrichon, Bâtiment Géode, 2 rue Raphaël Dubois, 69,622 Villeurbanne, France.
 Email: gwendal.perrichon@univ-lyon1.fr

Funding information

Agence Nationale de la Recherche, Grant/Award Number: ANR19-CE31-0006-01

Abstract

Voay robustus, the extinct Malagasy “horned” crocodile, was originally considered to be the only crocodylian representative in Madagascar during most part of the Holocene. However, Malagasy crocodylian remains have had confused taxonomic attributions and recent studies have underlined that *Crocodylus* and *Voay* populations coexisted on the island for at least 7500 years. Here, we describe the inner braincase anatomy of *Voay robustus* using x-ray computed tomography on four specimens, to provide new anatomical information that distinguishes *Voay* from *Crocodylus*, especially features of the brain endocast and the paratympenic sinuses. Geometric morphometric analyses are performed on 3D models of the internal organs to compare statistically *Voay* with a subset of extant Crocodylidae. Following these comparisons, we build an endocranial morphological matrix to discuss the proposed phylogenetic affinities of *Voay* with Osteolaeminae from an endocranial point of view. Additionally, we discuss the use of internal characters in systematic studies and find that they can have a major impact on morphological analyses. Finally, new radiocarbon data on *Voay* and subfossil *Crocodylus* specimens are recovered between 2010 and 2750 cal BP, which confirm the cohabitation of the two species in the same area for a long period of time. We thus assess several extinction scenarios, and propose a slightly different ecology of *Voay* compared to *Crocodylus*, which could have allowed habitat partitioning on the island. Our approach complements information obtained from previous molecular and morphological phylogenies, as well as previous radiocarbon dating, together revealing past diversity and faunal turnovers in Madagascar.

KEYWORDS

endocranial characters, Malagasy crocodylians, morphometry, neuroanatomy, paratympenic sinus, radiocarbon dating

This is an open access article under the terms of the [Creative Commons Attribution](https://creativecommons.org/licenses/by/4.0/) License, which permits use, distribution and reproduction in any medium, provided the original work is properly cited.

© 2023 The Authors. *The Anatomical Record* published by Wiley Periodicals LLC on behalf of American Association for Anatomy.

1 | INTRODUCTION

During the Holocene, the island of Madagascar has been home to two distinct species of crocodylids. One is still present nowadays and corresponds to an isolated population of the Nile crocodile, *Crocodylus niloticus*. The second, more enigmatic and now extinct, was the endemic Malagasy crocodile *Voay robustus* Grandidier & Vaillant, 1872. The taxonomy of this subfossil crocodylid was originally confused with regard to the genus *Crocodylus* (Angel, 1929; Barbour, 1918; Mook et al., 1921; Vaillant & Grandidier, 1910; White, 1930), until Brochu (2007) erected a neotype. *Voay* was then recovered in Osteolaeminae, as a sister-taxon to the African dwarf crocodile *Osteolaemus* (Figure 1a).

However, its phylogenetic position is currently debated, following the molecular study of Hekkala et al. (2021) on ancient DNA. Their analyses of partial mitochondrial genome extracted from *Voay* specimens retrieved the Malagasy genus as a stem-taxon to the genus *Crocodylus* (Figure 1b), thus interpreting its “osteolaemine” cranial characters as homoplastic. Later the same year, Rio and Mannion (2021) published a new morphological phylogenetic analysis of Crocodylia, which managed to reconcile the conflicting position of *Tomistoma* and *Gavialis* with the molecular analyses, and retrieved the original relationship of *V. robustus* with the extant dwarf crocodile *Osteolaemus*.

In fact, the phylogenetic positions of osteolaemine genera were already quite fragile: in particular, the

longirostrine genus *Mecistops* is systematically found clustered with *Crocodylus* in morphological topologies (Brochu, 2001, 2007; Delfino et al., 2020; Groh et al., 2019; Rio & Mannion, 2021), but is considered as an osteolaemine in molecular topologies (Harshman et al., 2003; Hekkala et al., 2011; Meredith et al., 2011; Oaks & Dudley, 2011; Pan et al., 2021). The “subfamily” Osteolaeminae thus seems to group morphologically distant taxa (†*Euthecodon*, †*Voay*, and †*Brochuchus*, see Rio & Mannion, 2021), whose phylogenetic congruence is now heavily questioned.

New evidence could come from endocranial characters, whose potential usefulness in taxonomy and phylogeny is now demonstrated (Kuzmin et al., 2021; Martin et al., 2022; Perrichon, Hautier et al., 2023). With the popularization of computed tomography techniques, large databases of internal morphological data can now be established to compare species statistically on a larger scale, in order to answer phylogenetic or ecological questions.

In this study, we propose to investigate the endocranial morphology of *V. robustus* by reconstructing its neurovascular and pneumatic structures. Our aim is to add new elements of comparison between this recently extinct species and its crocodyline and osteolaemine relatives, and discuss the use of endocranial morphology for taxonomy and phylogeny in the crocodylid framework. A complete description of endocranial structures is provided, and 3D geometric morphometric quantification of the sinuses was done to assess their morphological differentiation in Crocodylidae. Second, we test a new phylogenetic analysis of extant crocodylids, including *V. robustus*, using endocranial characters proposed in Kuzmin et al. (2021), and Perrichon, Hautier et al. (2023), as well as numerous newly defined characters, and further include them in a larger dataset of cranial features (Brochu et al., 2022). Additionally, we discuss potential palaeoecological implications of the differentiation of endocranial structures between *V. robustus* and *C. niloticus*, and bring along new radiocarbon measurements and compiled data from the literature, which together refine the modalities and timing of the temporal overlap of these two species in Madagascar during the Holocene.

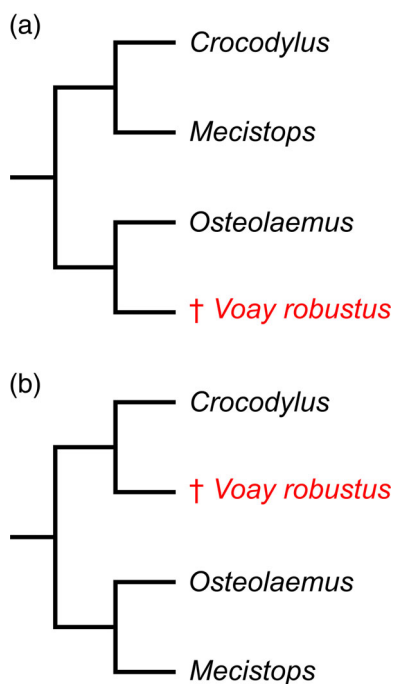


FIGURE 1 Current phylogenetic hypotheses of Crocodylidae. (a) Morphological hypothesis (Brochu, 2007; Rio & Mannion, 2021); (b) molecular hypothesis (Hekkala et al., 2021).

2 | MATERIALS AND METHODS

2.1 | Fossil specimens

Four specimens of adult *V. robustus* were examined in this study (Table 1): three from the Natural History Museum, London, UK (NHMUK PV R 36684, 36685, and 2204), and one from the Muséum National d'Histoire

TABLE 1 Information about the *Voay* specimens studied.

Specimen	Stratigraphic location	Locality	Date of retrieval	Retrieved by	Collection	Palaeoenvironment
NHMUK PV R 36684	Holocene	Ampoza	Probably 1930	cf. Data S1	Natural History Museum, London, UK	Flood plains
NHMUK PV R 36685	Holocene	Ampoza	Probably 1930	cf. Data S1	Natural History Museum, London, UK	Flood plains
NHMUK PV R 2204	Late Pleistocene	Itampulu-Vey	January 1984	Not specified	Natural History Museum, London, UK	Not specified
MNHN F.1908.5A	Holocene	Not specified	Not specified	Not specified	Muséum national d'Histoire naturelle, Paris, France	Not specified

Naturelle, Paris, France (MNHN F 1908.5A). The specimens NHMUK PV R 36684 and NHMUK PV R 36685 were collected near Ampoza, Madagascar (Figure 2), likely during the joint Franco-Anglo-American expedition that took place from 1927 to 1930 (Hekkala et al., 2021; White, 1930). These two specimens are beautifully preserved, with only slight damage to their left pterygoid, and half of the jugal of NHMUK PV R 36684 being missing (Figure 3a,b). The specimen NHMUK PV R 2204 is a complete braincase filled with a sandstone matrix, showing slight damage to the lateral part of the right otoccipital (Figure 3c). It was found near Itampulu-Vey, South-West Madagascar, in January 1984; however, we found no published reports of this location. The fourth specimen MNHN F 1908.5A is a near-complete skull with the left squamosal horn missing, and the left maxillary, premaxillary, lacrimal and jugal detached from the skull. It entered the collections in 1908, but no additional information was found on its discovery date or location.

2.2 | Surface scanning, x-ray CT, and production of 3D models

Surface scans were made to produce 3D models of the external surface of the skulls. It was done with the structured blue light Artec Space Spider 3D scanner (Artec 3D, Senningerberg, Luxembourg) for the NHMUK specimens, and with a white light Artec Eva 3D scanner for the MNHN specimen. Raw scans were then reconstructed using Artec Studio version 17 and exported in PLY format (Figure 3).

X-ray computed microtomography (μ CT) was used to scan the specimens and produce 3D models of the cranial internal structures (Figure 4). The three NHMUK specimens were scanned in January and March 2022 at the Natural History Museum of London using a Nikon XT H 225 ST. The specimen MNHN F 1908.5A was scanned in

2010 at Saint-Ouen-L'Aumône, Viscom France, using a X8060 NDT μ CT system. Raw CT data were imported into ImageJ (Schneider et al., 2012), where image stacks were converted from 16-bit to 8-bit and scaled down by a factor of two (binning $2 \times 2 \times 2$) to reduce file weight. Contrast was enhanced between bones, sediment infill and cavities, and files were exported in RAW format. All acquisition and post-processing parameters are provided in Table S1. Volume segmentation was performed in Avizo Lite (version 8.1 and 9.5), semiautomatically with the wand tool and manually with the brush tool, to create 3D volumes of the endocranial structures. Two-dimension images were captured in Avizo, and 3D mesh models were exported in PLY and STL format. All 3D models are available on MorphoMuseum (Perrichon, Pochat-Cottilloux et al., 2023, doi: <https://doi.org/10.18563/journal.m3.205>).

2.3 | Radiocarbon dating

Bone samples of MNHN F 1908.5A consisted of several small fragments; they were prepared for radiocarbon dating following the protocol detailed in Richardin et al., 2017. The samples were crushed, washed, and then powdered using a Fritsch Pulverisette 7. The resulting powder was treated with acetone and rinsed with water, then demineralized with hydrochloric acid to recover the collagen fraction. The obtained amount of collagen was sufficient to make two independent measurements. Radiocarbon measurements were done on the AMS facility of the Carbon 14 Measurement Laboratory (LMC14) at Saclay (France). Calibrated dates were calculated using the OxCal software v4.4.4 and the calibration data for the Southern Hemisphere SHCal20 (Hogg et al., 2020). Calibrated dates ranges are expressed in years cal BP (before 1950) and correspond to a probability interval depending on the sample (Table 2). The specimen MNHN F 1908.5B, a *Crocodylus* skull from Madagascar recently re-



FIGURE 2 Late Quaternary localities in Madagascar known to have produced remains of *Voay robustus*. Two of the specimens of this study come from the locality of Ampoza (indicated in red). Other reports are displayed in brown (Bickelmann & Klein, 2009; Brochu, 2007; Grandidier & Vaillant, 1872; Hekkala et al., 2021; Mook et al., 1921; Rakotozandry et al., 2021; Samonds et al., 2019).

discovered in the same drawer as the *Voay* specimen (i.e., MNHN F 1908.5A), was also dated for comparison following the same protocol.

2.4 | Comparative material

Three reference specimens were used for anatomical comparison of endocranial structures, chosen among adults at our disposal that were of comparable size with the *Voay* specimens (and the largest specimen available for *Osteolaemus*): *C. niloticus* MHNL 50001387, *Mecistops*

sp. UM N89, and *Osteolaemus tetraspis* UCBLZ 2019–1–236. Parameters used for μ CT of these specimens are provided in Table S1.

A total of 23 extant specimens were used in the geometric morphometric and phylogenetic analyses. Refer to Table 3 for a list of these specimens and their respective use in each of the analyses.

2.5 | Measurements and statistical analyses

Linear measurements were performed in Meshlab v2020.12. For volume calculation, we applied a “screened Poisson surface reconstruction” (Kazhdan & Hoppe, 2013) with “Pre-clean” activated on the non-manifold meshes, to transform them into watertight volumes. Volume measurements were then calculated both with Meshlab and Blender 2.92 to avoid possible scale errors.

Three-dimension geometric morphometric quantification was performed on the pharyngotympanic sinuses of the four *Voay* specimens and 17 extant adult Crocodylidae (Table 3). The right side of each 3D model was characterized by a set of 31 landmarks, comprising a combination of type I and type II landmarks. Landmark locations were chosen to match the intersection between the different sinus cavities, and to reflect the shape and extension of these recesses (Table S2 and Figure S14). They were placed on the 3D models using Morphodig 1.6.4 following a similar protocol as in Perrichon, Hautier et al. (2023), and exported in TPS format.

A similar protocol was applied to the left side of the brain endocast of this dataset, this time using 22 landmarks, except from one specimen, UM N89, which lacks the anterior part of the brain endocast (Table S3 and Figure S15).

All analyses were performed in R 4.2.1 (R Core Team, 2021), using functions from geomorph 4.0.4 (Adams et al., 2022). Raw landmark coordinates were transformed using a generalized least-squares Procrustes analysis with *gpagen* to correct for size and alignment of specimens. A principal component analysis (PCA) was performed on the Procrustes shape coordinates with *gm.prcomp* to find the major axes of shape variation within our dataset. *plotRefToTarget* was used to create 3D wireframes of the pharyngotympanic sinus to visualize the shape modifications between the mean shape and extreme values of the PC axes, respectively calculated with *mshape* and *shape.predictor*.

Evaluation of size effects and impact of phylogenetic classes on total shape and PC axes was performed using Procrustes ANOVA (equivalent to a Permutational Multivariate Analysis of Variance, Anderson, 2001) on the

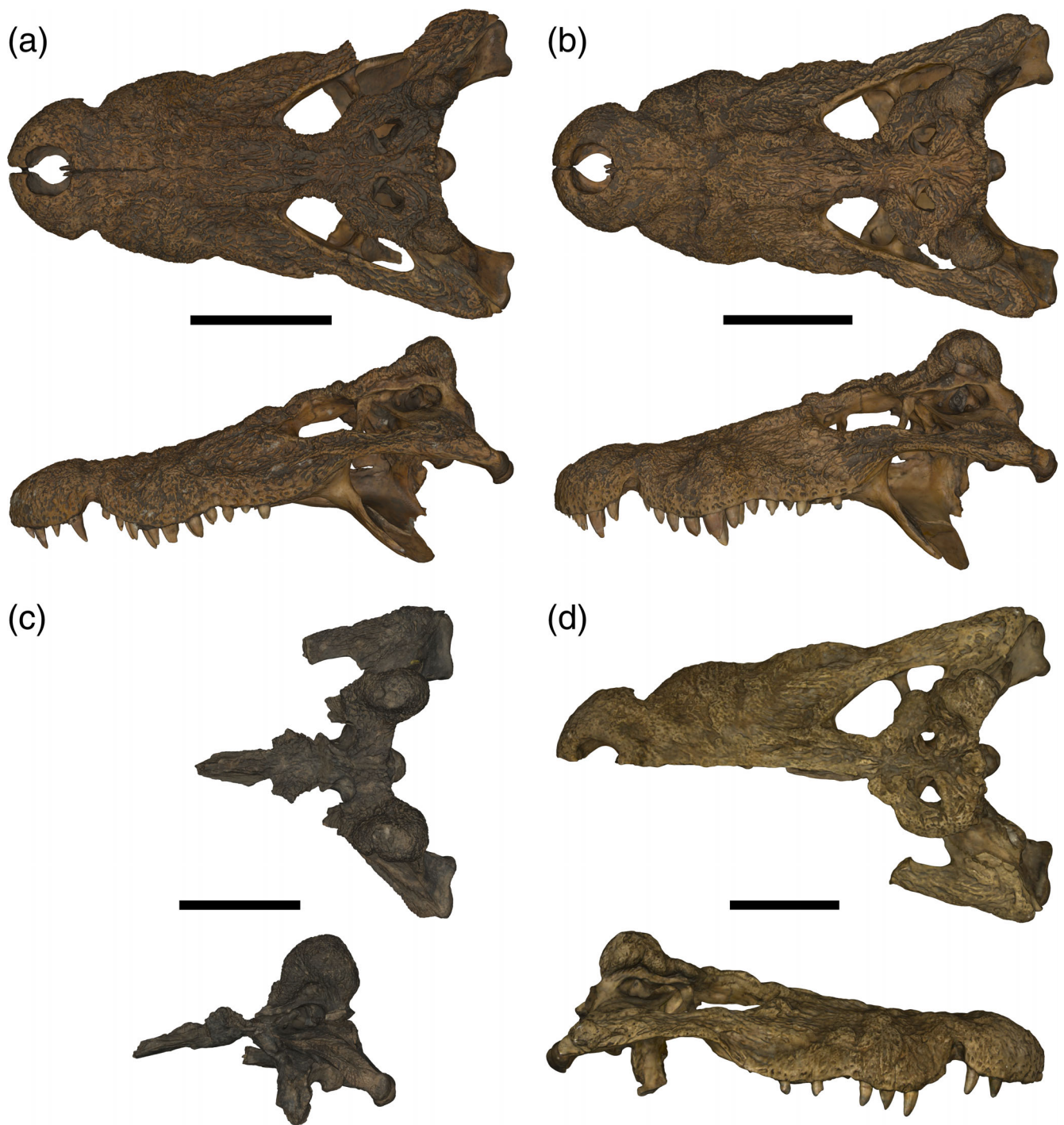


FIGURE 3 External 3D views of *Voay robustus* specimens studied. (a) NHMUK PV R 36684, (b) NHMUK PV R 36685, (c) NHMUK PV R 2204 in dorsal (top) and left lateral view (bottom); (d) MNHN F 1908.5A in dorsal (top) and right lateral view (bottom). Scale bars equals 10 cm.

Procrustes shape coordinates and PC scores with *procD.lm*. Influence of size on the morphospace resulting from the PCA was controlled using *plotAllometry* with the method “common allometric component (CAC),” to extract the CAC of shape and analyze the residual shape components (RSC) without the influence of size. Pairwise comparisons of the means and variances of each genus were done using *pairwise*.

Data visualization was performed using *plot3d*, and *ggplot* from the *ggplot2* 3.3.6 package (Wickham, 2011).

2.6 | Phylogenetic analyses

Characters were reviewed on the brain endocast, endosseous labyrinth and paratympanic sinuses. These

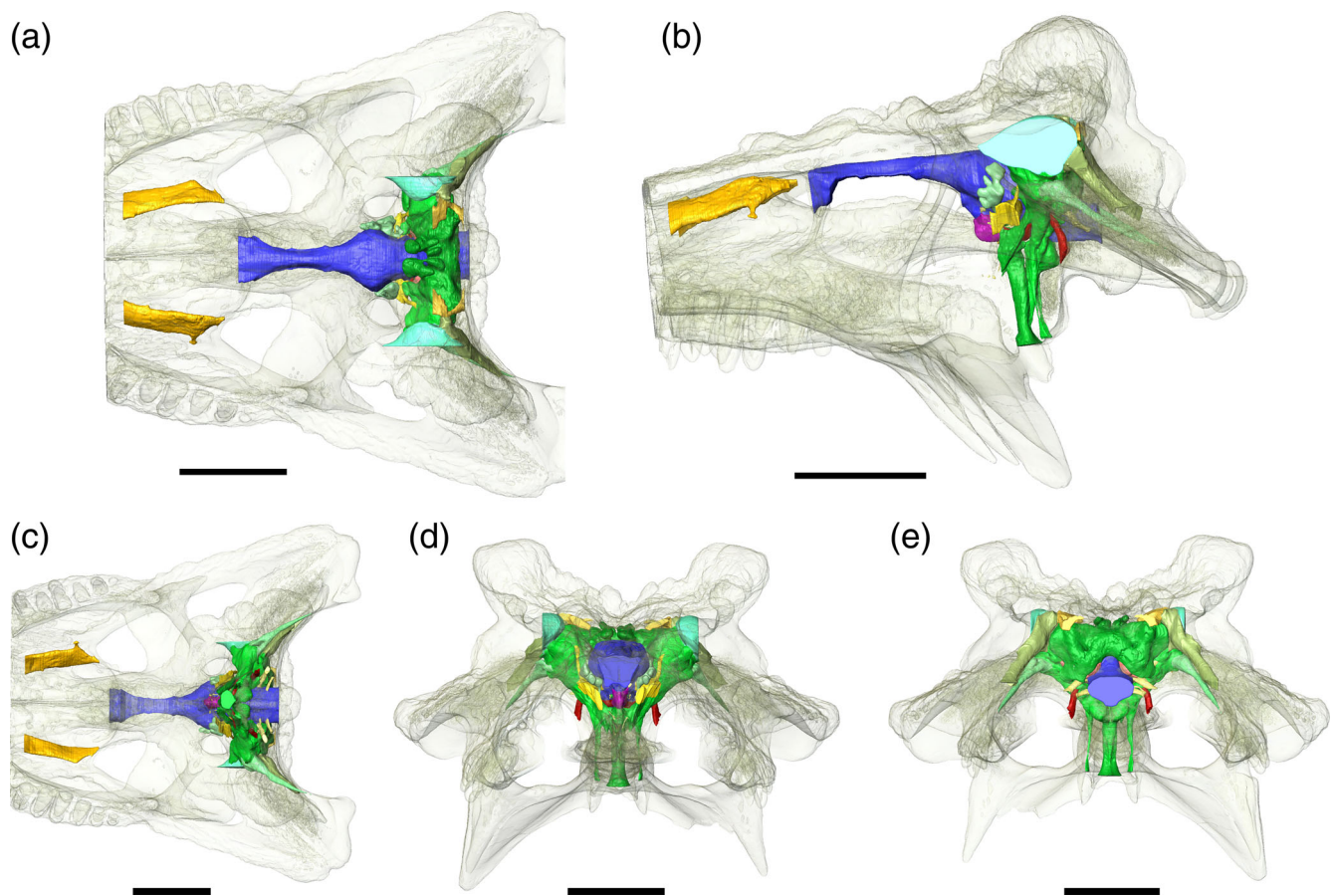


FIGURE 4 Transparent 3D reconstruction of the rear skull of *Voay robustus* NHMUK PV R 36685 showing the endocranial elements. (a) Dorsal; (b) left lateral; (c) ventral; (d) anterior; (e) posterior views. Scale bars equals 5 cm.

TABLE 2 Radiocarbon ages (BP) and calibrated dates (cal BP) obtained for the bone samples of *Voay* (MNHN F.1908.5A) and *Crocodylus* (MNHN F. 1908.5B).

Specimen	Reference	Lab. Code	^{14}C age BP	Calibrated date 2σ (95.4%) cal BP
MNHN F. 1908.5A	1A2007	SacA69477	2110 \pm 30	2120 (86.1%) 1990 cal BP
				1970 (9.4%) 1930 cal BP
	2A2007	SacA69478	2190 \pm 30	2310 (28.1%) 2230 cal BP
				2160 (65.0%) 2040 cal BP
	Comb.		2150 \pm 22	2290 (0.9%) 2270 cal BP 2140 (94.5%) 2000 cal BP χ^2 -test: df = 1 T = 3.6 (5% 3.8)
MNHN F. 1908.5B	1A2008	SacA69479	2570 \pm 30	2750 (95.4%) 2480 cal BP
				2750 (95.4%) 2480 cal BP
	2A2008	SacA69480	2565 \pm 30	2750 (95.4%) 2480 cal BP
				2750 (95.4%) 2480 cal BP
	Comb.		2538 \pm 22	2750 (30.2%) 2670 cal BP 2660 (65.2%) 2490 cal BP χ^2 -test: df = 1 T = 0.0 (5% 3.8)

Note: Each specimen has two duplicates and one combined result (in bold) checked for internal consistency by a Chi-squared test.

endocranial characters were then discretized and used in cladistic analyses. We used 19 specimens representing 10 species of Crocodylidae including *Crocodylus acutus*,

C. halli, *C. intermedius*, *C. niloticus*, *C. palustris*, *C. porosus*, *C. siamensis*, *Mecistops* sp., *Osteolaemus tetraspis*, and *V. robustus*. One specimen of *Alligator*

TABLE 3 List of specimens used in this study as comparative material.

Species	ID	Provider	Analyses involved
<i>Alligator mississippiensis</i>	MHNL 50001401	Musée des Confluences, Lyon	P
<i>Crocodylus acutus</i>	MZS Cro 055	Musée Zoologique de Strasbourg	M, P
<i>Crocodylus halli</i>	UF herp 145927	UF Nanoscale research facility (Morphosource)	M, P
<i>Crocodylus intermedius</i>	MNHN ZA AC 1885–489	Muséum National d'Histoire Naturelle, Paris	P
<i>Crocodylus niloticus</i>	UCBL FSL 532077	Collections de Géologie UCBL	M
<i>Crocodylus niloticus</i>	UM 2001–1756-1-434NR	Université de Montpellier	M
<i>Crocodylus niloticus</i>	MHNL 50001388	Musée des Confluences, Lyon	M, P
<i>Crocodylus niloticus</i>	MHNL 50001387	Musée des Confluences, Lyon	D, M, P
<i>Crocodylus niloticus</i>	MHNL 50001405	Musée des Confluences, Lyon	P
<i>Crocodylus palustris</i>	MHNL 50001398	Musée des Confluences, Lyon	P
<i>Crocodylus porosus</i>	MHNL 50001402	Musée des Confluences, Lyon	P
<i>Crocodylus siamensis</i>	UCBLZ 2019–1-237	Collections de Zoologie UCBL	M
<i>Crocodylus siamensis</i>	MHNL 50001389	Musée des Confluences, Lyon	M, P
<i>Crocodylus siamensis</i>	UCBLZ WB41	Collections de Zoologie UCBL	M, P
<i>Mecistops cataphractus</i>	NHMUK 1924.5.10.1	Natural History Museum, London	P
<i>Mecistops</i> sp.	SVSTUA 022001	Collections de l'Agrégation de l'ENS de Lyon	M
<i>Mecistops</i> sp.	MHNL 50001393	Musée des Confluences, Lyon	M
<i>Mecistops</i> sp.	AMU Zoo-04721	Aix-Marseille Université	M
<i>Mecistops</i> sp.	UM N89	Université de Montpellier	D, M, P
<i>Osteolaemus tetraspis</i>	MNHM 9095–0	Muséum d'Histoire Naturelle de Marseille	M
<i>Osteolaemus tetraspis</i>	MZS Cro-040	Musée Zoologique de Strasbourg	M, P
<i>Osteolaemus tetraspis</i>	NHMUK 1862.6.30.5	Natural History Museum, London	M, P
<i>Osteolaemus tetraspis</i>	UCBLZ 2019–1-236	Collections de Zoologie UCBL	D, M, P

Abbreviations: D, comparative description; M, geometric morphometric analysis; P, Phylogenetic analysis.

mississippiensis was chosen as the operational outgroup. Characters were scored on 3D models and tomograms; they were chosen based on interspecific variations of the shape of internal organs, and optimized to include minimal ontogenetic variations. Given that our aim was to evaluate the impact of characters scored on endocranial organs (i.e., their impression on the internal surface of the braincase bones), only this type of character was included at first.

All analyses were carried out on TNT v.1.6 (Goloboff & Morales, 2023) using implicit enumeration. Resampling was done with a standard bootstrap procedure on the consensus topology with 1000 replicates using traditional search.

Two consecutive parsimony analyses were made to test chosen characters. First, a preliminary analysis was performed using a matrix of 25 discrete characters and 20 specimens as operating taxa (Data S6). This analysis was made to confirm whether chosen characters were stable across several adult specimens of a single species, and if the chosen characters were able to cluster specimens from the same species and genus. A few of these

characters were found to be already mentioned in previously published phylogenetic analyses, including Brochu (1997); Rio and Mannion (2021); and Kuzmin (2022) (see Data S3 and S8). These characters were tested anyway using the same methods.

This first analysis led us to reconsider the initial matrix, in which we pruned several characters: some that were intraspecifically variable and others that indirectly defined the volume of the recesses, with the aim to reduce the convergence of our internal character matrix with rostrum shape and refine the relationships between species (see the Discussion section). Uninformative characters were also removed to avoid unnecessary weight (i.e., character 20 of the preliminary analysis, “intertympanic recess,” coded as “present, fully developed” in all studied specimens of Crocodylia). The complete list of characters removed between the first and second analysis can be found in the Data S3.

Species were used as operating taxa for the second analysis, defined as operational taxonomic units (OTU) grouping the previous specimens under the condition that the

remaining characters were seemingly stable across all specimens of a same species. This resulted in 11 OTU. This second analysis was thus performed using a matrix of 15 discrete characters and 11 taxa (Data S7 and S8). As nothing is known for now about the polarity of these endocranial characters, all character states were treated as unordered.

Finally, to evaluate the impact of these internal characters on an already existing topology, we included our matrix in a larger, more comprehensive dataset. We used the morphological character matrix of Brochu et al. (2022), selecting only the taxa used in our study (Data S9). To make these results comparable with our previous matrix, we rooted the tree using *Alligator mississippiensis*, using the character states for this taxa scored in Brochu (2012), which uses the same 189 characters; we then coded the 6 additional characters created in Brochu et al. (2022) using the specimen of *Alligator mississippiensis* MHNL 50001401 at our disposal. *Crocodylus novaeguineae* was here considered as equivalent to *Crocodylus halli* in terms of character coding, as the two species were only distinguished from each other very recently (Murray et al., 2019).

2.7 | Institutional abbreviations

AMU: Aix-Marseille Université, Marseille, France.

MHNL: Musée d'Histoire Naturelle de Lyon, Lyon, France.

MNHM: Muséum d'Histoire Naturelle de Marseille, Marseille, France.

MNHN: Muséum National d'Histoire Naturelle, Paris, France.

MZS: Musée Zoologique de Strasbourg, Strasbourg, France.

NHMUK: Natural History Museum of the United Kingdom, London, UK.

SVSTUA: Collections de l'Agrégation de l'ENS de Lyon, Lyon, France.

UCBL: Université Claude Bernard Lyon 1, Villeurbanne, France.

UF: University of Florida, Florida Museum of Natural History, Gainesville, USA.

UM: Université de Montpellier, Montpellier, France.

3 | SYSTEMATIC PALAEOLOGY

Crocodylia (Owen, 1842).

Crocodylidae (Cuvier, 1807).

Osteolaeminae (Brochu, 2003).

Voay Robustus (Grandidier & Vaillant, 1872).

Neotype: MCZ 1006, skull (Museum of Comparative Zoology, Cambridge, USA).

Occurrence: Upper Pleistocene to Late Holocene, Madagascar.

Referred material: MNHN F.1908.5A, skull; NHMUK PV R 2204, partial skull; NHMUK PV R 36684, skull; NHMUK PV R 36685, skull.

Diagnosis: see Brochu (2007).

Emended diagnosis: original diagnosis, plus square-shaped pituitary fossa oriented vertically; unpaired post-carotid recess developed in adult stages, protruding from the dorsal roof of the basisphenoid recess; bulbous quadrate recess developed posterolaterally, coalescent with an enlarged siphonium. Combination of: spade-shaped cerebrum in dorsal view; anteroposteriorly large midbrain with protruding optic lobes; vertical median pharyngeal canal of constant or increasing thickness; dorsally developed laterosphenoid recess connected to *recessus epitubaricus*; posteriorly inflated basioccipital recess; bulbous prootic facial recess developed anteriorly; intertympanic recess with an anteriorly developed prootic part.

Remarks: the affiliation of *Voay* to the subfamily Osteolaeminae is currently debated. It is here affiliated to the Osteolaeminae following all recent morphological phylogenetic hypotheses where it is included (Brochu et al., 2022; Kuzmin, 2022; Rio & Mannion, 2021). However, one molecular data analysis suggests that *Voay* has more affinities with the genus *Crocodylus* rather than *Osteolaemus* (Hekkala et al., 2021), making its true affinities still uncertain.

4 | NEUROANATOMICAL AND PNEUMATIC DESCRIPTION

4.1 | Brain endocast

A complete reconstruction of the brain endocast was possible for NHMUK PV R 36684 and NHMUK PV R 36685 (Figure 3a and 3b). NHMUK PV R 2204 (Figure 3c) lacks the olfactory bulb, and the entire olfactory apparatus could not be reconstructed in MNHN F 1908.5A (Figure 3d) as these regions could not be reached by the sample manipulator of the μ CT instrument. Measurements of the brain endocast on the four specimens are given in Table 4. The brain endocast is bounded anteriorly by the prefrontal pillars that support the olfactory bulb (Figure 5); dorsally by the frontal, parietal, supraoccipital, and otoccipital; laterally by the laterosphenoids, prootics and otoccipitals; and ventrally by the basisphenoid and basioccipital. As in other Crocodylia representatives, the endocast is sigmoidal in lateral view. In *Voay*, it shows a pronounced posterior curve, with marked cephalic (129° – 140°) and pontine (130° – 139°) flexure

TABLE 4 Endocranial measurements of the brain endocast, endosseous labyrinth and paratympanic recesses of the four specimens studied.

	NHMUK PV R 36684	NHMUK PV R 36685	NHMUK PV R 2204	MNHN F 1908.5A	Mean
Endocast					
Cephalic flexure angle (°)	138.0	129.0	130.0	140.0	134.3
Pontine flexure angle (°)	138.0	130.0	130.0	139.0	134.3
Brain endocast (length)	111.0	113.0	>112	>80	112.0
Olfactory apparatus (length)	54.0	53.0	>48	NA	53.5
Olfactory apparatus, % of total length	48.6	46.9	>43	NA	47.8
Olfactory bulbs (width)	22.0	23.0	NA	NA	22.5
Cerebral hemispheres (width)	34.0	32.0	34.0	32.0	33.0
Cerebral hemispheres (height)	23.0	24.0	23.0	23.0	23.3
Midbrain region (width)	20.0	19.0	19.0	20.0	19.5
Midbrain region (length)	7.0	7.0	8.5	9.0	7.9
Midbrain region (height)	24.0	26.0	29.0	27.0	26.5
Hindbrain region (width)	22.0	23.0	25.0	25.0	23.8
Hindbrain region (height)	30.0	32.0	30.0	30.0	30.5
Medulla oblongata (length)	8.0	9.0	13.6	12.0	10.7
Pituitary fossa (length)	13.0	11.0	>7	>7	12.0
Pituitary fossa (width)	4	6.0	8.0	8.0	7.3
Pituitary fossa (height)	13.0	11.0	11.0	15.0	12.5
Endosseous labyrinth					
Total anteroposterior length	15.3	16.8	17.0	17.1	16.6
Total height	21.6	21.0	19.7	22.5	21.2
Vestibular apparatus (height)	11.6	12.3	11.4	12.8	12.0
Common crus (height)	3.1	3.3	3.3	3.1	3.2
Cochlear duct (height)	11.5	10.7	8.8	11.8	10.7
Cochlear duct (width)	2.0	2.1	1.8	2.2	2.0
<i>Fenestra ovalis</i> (height)	3.1	3.2	3.4	3.0	3.2
<i>Fenestra ovalis</i> (length)	5.8	5.9	6.9	6.1	6.2
Angle between anterior and posterior semicircular canals (°)	88.0	87.0	94.0	101.0	92.5
Angle between anterior and lateral semicircular canals (°)	45.0	44.0	39.0	36.0	41.0
Angle between posterior and lateral semicircular canals (°)	49.0	47.0	50.0	46.0	48.0
Paratympanic sinuses					
Total height	75.6	84.7	90.5	91.2	85.5
Median pharyngeal canal (height)	22.5	29.5	39.3	28.4	29.9
Ostium of the median pharyngeal canal (width)	7.0	9.2	7.9	6.0	7.5
Median pharyngeal canal, maximum width	5.3	7.7	8.9	9.0	7.7
Basioccipital part of the median pharyngeal canal, maximum width	5.8	7.5	7.9	8.4	7.4
<i>Recessus epitubaricus</i> (height)	23.9	19.3	20.7	17.0	20.2
Basioccipital recess (width)	11.8	10.3	7.8	10.0	9.9

(Continues)

TABLE 4 (Continued)

	NHMUK PV R 36684	NHMUK PV R 36685	NHMUK PV R 2204	MNHN F 1908.5A	Mean
Rhomboidal recess, anteroposterior width	6.0	7.3	9.0	8.2	7.6
Pharyngotympanic tubes (height)	23.0	31.0	33.0	NA	29.0
Pharyngotympanic tubes (width)	1.0	3.6	3.2	NA	2.6
Canal to laterosphenoid recess (width)	3.0	1.3	0.5	1.0	1.4
Laterosphenoid recess (height)	19.4	20.6	18.2	23.4	20.4
Subtympanic foramen (width)	7.7	5.1	6.9	6.2	6.5
Subtympanic foramen (length)	3.8	3.6	3.7	4.1	3.8
Siphonium, starting width	3.7	4.5	3.2	3.8	3.8
Siphonium, foramina width	1.8	0.6	1.6	NA	1.3

Note: Units are in mm. Bold values correspond to the mean values of each measurement.

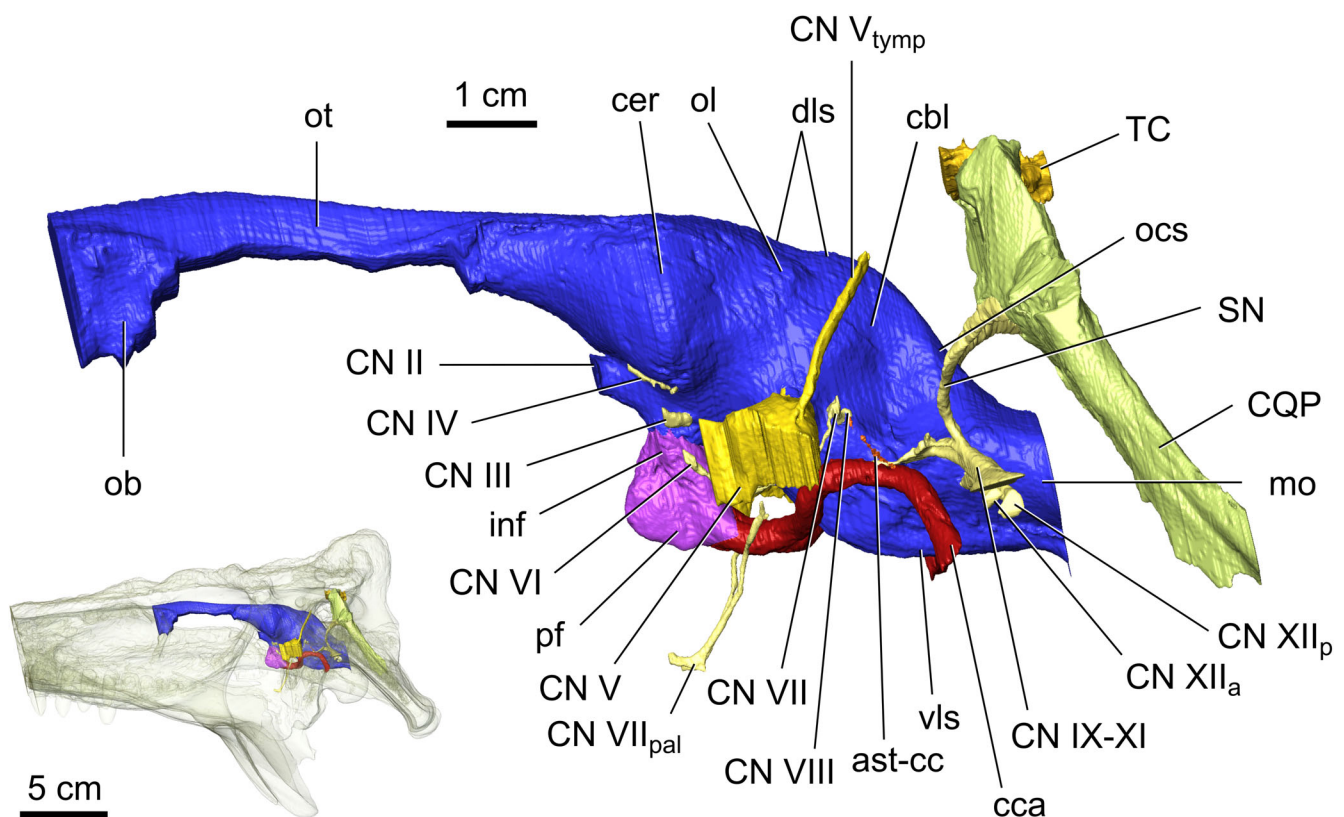


FIGURE 5 Left lateral view of the neurovascular system of *Voay robustus* NHMUK PV R 36684. Bottom left corner: left lateral view of the posterior part of the skull rendered transparent showing the location of the internal structures. ast-cc, arterial branch between stapedial and cerebral carotid arteries; cbl, cerebellum; cca, cerebral carotid arteries; cer, cerebral hemispheres; CN II, optic nerve; CN III, oculomotor nerve; CN IV, trochlear nerve; CN V, trigeminal nerve; CN V_{tymp}, tympanic branch of trigeminal nerve; CN VI, abducens nerve; CN VII, facial nerve; CN VII_{pal}, palatine branch of facial nerve; CN VIII, vestibulocochlear nerve; CN IX-XI, common canal for glossopharyngeal, vagus and spinal accessory nerve; CN XII_a, anterior hypoglossal nerve; CN XII_p, posterior hypoglossal nerve; CQP, cranioquadrate passage; dls, dorsal longitudinal venous sinus; inf, infundibulum; mo, medulla oblongata; ob, olfactive bulb; ocs, otoccipital venous sinus; ol, optic lobe; ot, olfactive tract (CN I); pf, pituitary fossa; SN, sympathetic nerve; TC, temporal canal; vls, ventral longitudinal venous sinus.

angles. This sigmoid is similar to the shape of the *Osteolaemus* endocast, compared to the lighter curve observed

in other Crocodylidae (Figure 14). The dorsal contour of the brain endocast is rather straight from the olfactory

bulb to the midbrain; it is slightly depressed ventrally between the olfactory tract and the cerebrum and inflates slightly dorsally at the level of the cerebrum (Figure 5). The dorsal longitudinal venous sinus displays a weak or absent depression above the midbrain, remaining straight when entering the hindbrain, then drops abruptly over the cerebellum, joining the otoccipital venous sinus (ocs, Figures 6 and 7). The posterior part of the endocast has a straight shape over the metencephalon where the brain exits the skull posteriorly via the medulla oblongata, through the foramen magnum.

The anterior part of the forebrain includes the olfactory bulbs and the olfactory tracts, and represents almost 50% of the total length of the endocast. The olfactory bulbs are bounded by the prefrontal pillars at the anterior tip of the brain, whereas the olfactory tract is bounded dorsally by the frontal until the anterior-most part of the laterosphenoids. The endocast of the olfactory bulbs is large, representing 68% of the width at the cerebral hemispheres (~2.3 mm, Table 4), and ~80% of their height. It is positioned at the same dorso-ventral level than the cerebral hemispheres, as in *Crocodylus* and *Mecistops*, but contrary to *Osteolaemus* where it occupies a more ventral position. A median sulcus is visible in dorsal view between the left and right olfactory bulbs (Figure 6). The olfactory tract links the cerebral hemispheres into the olfactory bulbs. It is wider at the level of the laterosphenoids and above the prefrontal pillars. The olfactory tract of *V. robustus* shows a straight profile with a subtle dorsal inclination, and a slight dorsal curvature until it joins the olfactory bulbs, at around three quarters of its length from the cerebrum. It attains its narrowest point at around 60% of its length from the cerebrum.

The widest portion of the brain endocast sits at the level of the cerebral hemispheres, or cerebrum, which forms the posterior part of the forebrain. The cerebrum forms two rounded lateral bulges, tapering toward the olfactory tract anteriorly. Each hemisphere shows an acute spade-shape in dorsal view, in comparison with the more rounded lateral surfaces observed in extant Crocodylidae. Their dorsal surface is flat, whereas their ventral parts are curved ventrally over the root of the optic nerve (CN II, Figure 5).

Ventrally to the cerebrum and the oculomotor nerve (CN III), the infundibulum is characterized by a pair of laterally inflated bulges marking the ventral-most part of the forebrain and the limit between the latter and the pituitary fossa (inf, Figure 5). Ventrally to this area lies the pituitary (or hypophyseal) fossa, enclosed in the basisphenoid, where the paired cerebral carotid arteries connect to the brain. The pituitary

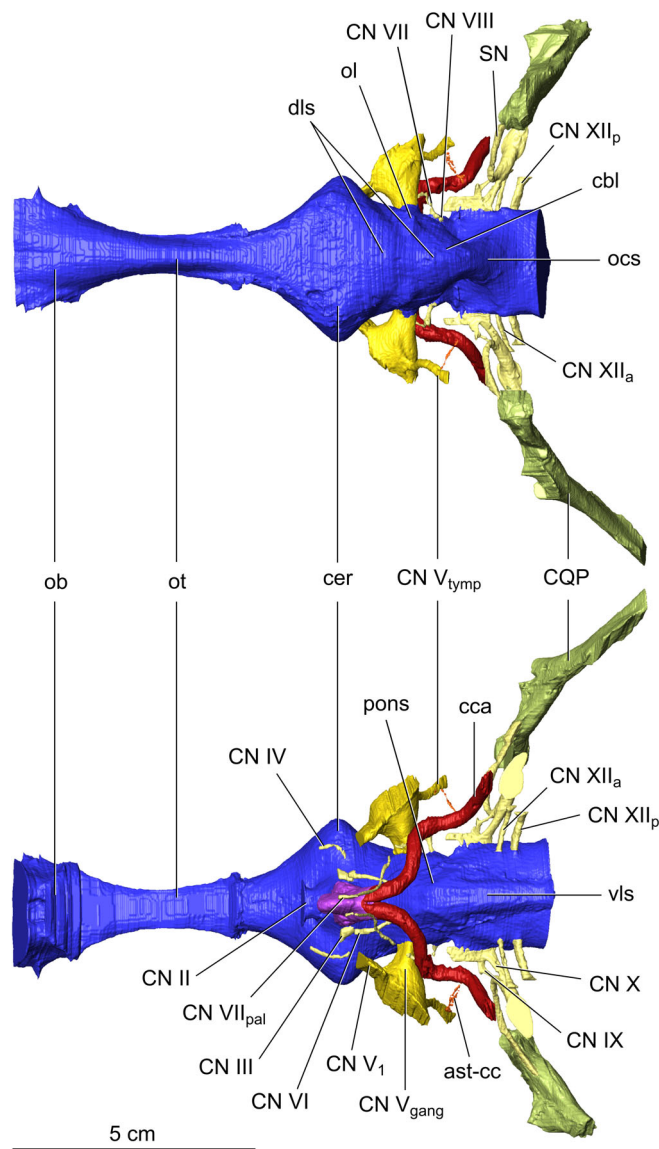


FIGURE 6 Dorsal (top) and ventral (bottom) views of the neurovascular system of *Voay robustus* NHMUK PV R 36684. The temporal canal has been removed for visualization purposes. ast-cc, arterial branch between stapedial and cerebral carotid arteries; cbl, cerebellum; cca, cerebral carotid arteries; cer, cerebral hemispheres; CN II, optic nerve; CN III, oculomotor nerve; CN IV, trochlear nerve; CN V₁, ophthalmic nerve; CN V_{gang}, ganglion of the trigeminal nerve; CN V_{tymp}, tympanic branch of trigeminal nerve; CN VI, abducens nerve; CN VII, facial nerve; CN VII_{pal}, palatine branch of facial nerve; CN VIII, vestibulocochlear nerve; CN IX, glossopharyngeal nerve; CN X, vagus nerve; CN XII_a, anterior hypoglossal nerve; CN XII_p, posterior hypoglossal nerve; CQP, cranioquadrate passage; ob, olfactory bulb; ocs, otoccipital venous sinus; ol, optic lobe; ot, olfactory tract (CN I); pf, pituitary fossa; SN, sympathetic nerve; vls, ventral longitudinal venous sinus.

fossa of *Voay* is oriented ventrally, and associated with a cavity that protrudes anteriorly and ventrally, showing a squared profile in lateral view, a shape unseen in

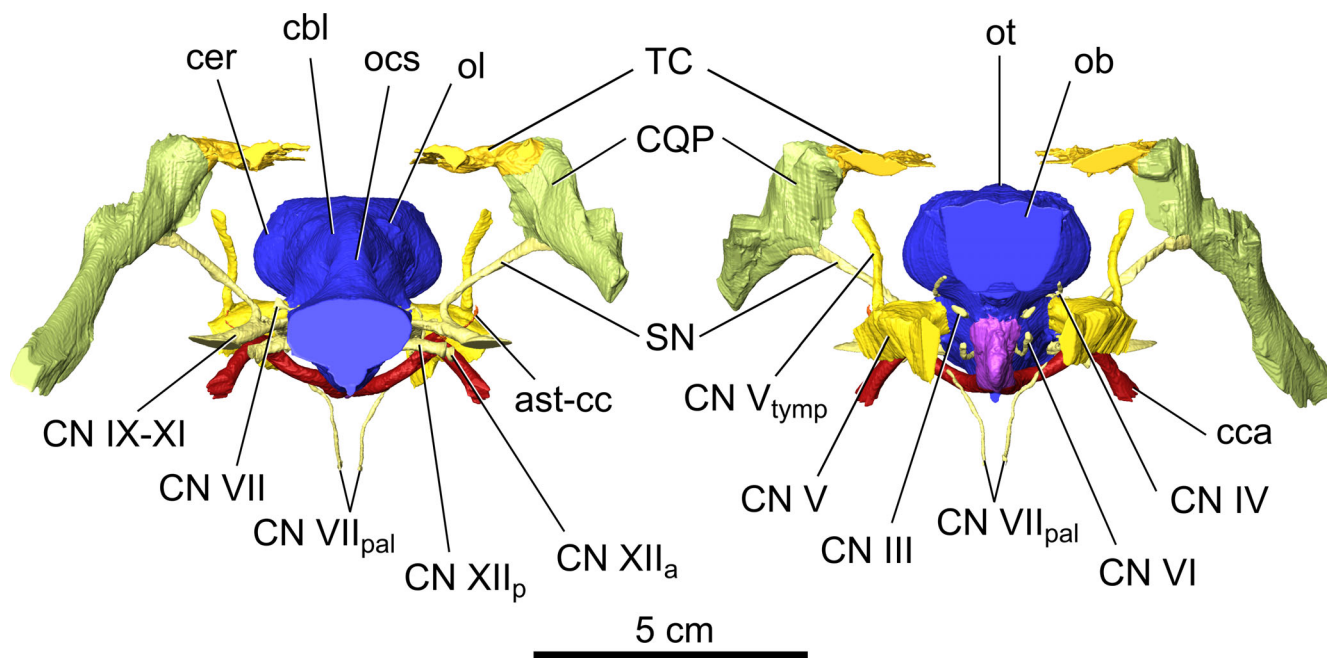


FIGURE 7 Posterior (left) and anterior (right) views of the neurovascular system of *Voay robustus* NHMUK PV R 36684. ast-cc, arterial branch between stapedia and cerebral carotid arteries; cbl, cerebellum; cca, cerebral carotid arteries; cer, cerebral hemispheres; CN III, oculomotor nerve; CN IV, trochlear nerve; CN V, trigeminal nerve; CN V_{tymp}, tympanic branch of trigeminal nerve; CN VI, abducens nerve; CN VII_{pal}, palatine branch of facial nerve; CN IX-XI, common canal for glossopharyngeal, vagus and spinal accessory nerve; CN XII_a, anterior hypoglossal nerve; CN XII_p, posterior hypoglossal nerve; CQP, cranioquadrate passage; dls, dorsal longitudinal venous sinus; ob, olfactory bulb; ocs, otoccipital venous sinus; ol, optic lobe; ot, olfactory tract (CN I); SN, sympathetic nerve; TC, temporal canal.

any other extant species (Figure 5). The canals for the cerebral carotid arteries are attached posteriorly to the pituitary fossa.

Posterodorsally to the cerebrum, the brain endocast inflates slightly, hiding the dorsal junction between the hindbrain and the midbrain and marking the dorsal longitudinal venous sinus (dls). It is wide anteriorly to the midbrain, being ~50% of the width of the cerebral hemispheres, and reduces laterally between the optic lobes (Figure 6). In large specimens, the dorsal longitudinal venous sinus is more inflated dorsally (MNHN F 1908.5A) and largely overlaps the midbrain (NHMUK PV R 2204).

The midbrain region is located posteriorly to the cerebral hemispheres and anteriorly to the cerebellum and the trigeminal nerve (CN V). As is generally the case in crocodylians, it is the smaller area of the brain. Here, the midbrain of *V. robustus* is 7–9 mm in length, which represents ~7% of the total brain endocast length, against ~5% in compared Crocodyliidae. Its width is ~60% of the cerebrum width. The midbrain hosts the optic lobes (or tectum), whose impressions on the endocast surface are very prominent in *V. robustus*. They are located on each laterodorsal part of the midbrain and protrude laterodorsally 1–2 mm from the surface of the endocast (Figures 5–7).

The metencephalon (anterior part of the hindbrain) hosts the cerebellum dorsally and the pons ventrally (anteroventral portion of the hindbrain connecting the medulla to the forebrain, see Figure 6). Here, the presence of the cerebellum is visible as a slight dorsal bulge on the dorsal outline of the endocast, anteriorly to the abrupt descent of the otoccipital venous sinus toward the medulla. Just posteroventrally to the cerebellum, the brain endocast is constricted mediolaterally where it accommodates for the otic bulla, that is, the bone complex formed by the prootic, supraoccipital, and otoccipital that hosts the endosseous labyrinth of the inner ear. The large foramen for the trigeminal nerve (CN V) lies anteriorly to the otic bulla.

A prominent longitudinal swelling of the endocast lies ventral to the hindbrain; it corresponds to the ventral longitudinal venous sinus (vls), which runs from the level of cranial nerve V to the posterior end of the myelencephalon (Figures 5 and 6). It is narrow and ventrally prominent compared to the larger and flatter profile of the vls of *C. niloticus*. It is larger anteriorly (~8.5 mm in width) and slightly tapers posteriorly to the medulla, reaching a width of 5.5 mm at the level of the foramen magnum.

The myelencephalon (posterior portion of the hindbrain) contains the medulla oblongata, bounded dorsally

by the otoccipital venous sinus and ventrally by the ventral longitudinal venous sinus. It has an oval shape in transverse view, is flattened dorsally, and connects the brain to the spinal cord through the foramen magnum (Figure 7). In *V. robustus*, the myelencephalon is short compared to the total length of the brain (7.5%–9.5% of total endocast length).

4.2 | Cranial nerves

All cranial nerves could be reconstructed to a certain extent in NHMUK PV R 36684. In NHMUK PV R 2204, the anteroventral part of the laterosphenoids is broken, which hides the root of cranial nerve II. In MNHN F 1908.5A, the cranial nerve I (olfactory tract) is absent from the scanned area (Figures 5–7).

The root of the optic nerve, or cranial nerve II (CN II), emerges ventrally to the cerebral hemispheres and joins the orbital cavity through a foramen bounded by the anteroventral parts of the laterosphenoids. This nerve is encapsulated in the bone at the start of its course, in an oval and large canal around 6 mm wide, in the anteroventral part of the laterosphenoids (Figures 5 and 6).

The canal for the oculomotor nerve or cranial nerve III (CN III) emerges on the lateral surface of the endocast, ventrally to the cerebral hemispheres and dorsally to the infundibulum (Figure 5). It is short (~3 mm) and runs anterolaterally, dorsally to the laterosphenoid–basisphenoid suture, going out of the skull in the posteroventral side of the orbital cavity.

The trochlear nerve, or cranial nerve IV (CN IV), is a very thin canal of constant thickness (7–8 mm in diameter), around 8 mm long, which emerges on the ventral surface of the cerebral hemisphere (Figure 5). It runs through the laterosphenoids, following the curvature of the cerebrum, before entering the posterior part of the orbital cavity.

The trigeminal nerve complex or cranial nerve V (CN V) is the largest neurovascular structure connecting to the brain. It exits the anterior part of the hindbrain through the trigeminal foramen (ø 5 mm), and then expands into the trigeminal fossa, a large bulbous cavity situated laterally to the endocast (ø 8 mm). This fossa is anteriorly bounded by the laterosphenoids, posteromedially by the prootic, and posterolaterally by the quadrate; it hosts the trigeminal ganglion (CN V_{gang}). Four major nerve canals are supposed to be rooted in the trigeminal ganglion: the ophthalmic, maxillary, mandibular, and tympanic branches (George & Holliday, 2013; Lessner & Holliday, 2020). The first three branches could not be reconstructed properly, as they are not included in bones. Only the bony groove hosting the root of the ophthalmic branch could be segmented (CN V₁,

Figure 6). It is dorsoventrally high, located anteroventrally to the trigeminal ganglion, and directed anteriorly. The tympanic branch of the trigeminal nerve is complete in all specimens; it emerges from the trigeminal ganglion posterodorsally (CN V_{tym}, Figures 5 and 6). Its canal is around 2 mm thick and 15–18 mm long, directed mainly dorsally and slightly posteriorly through the prootic. It follows the suture between the latter and the quadrate, before entering the ceiling of the pharyngotympanic sinus just anteromedially to the tympanic membrane.

The abducens nerve, or cranial nerve VI (CN VI), emerges from the ventral side of the midbrain and runs through the anterior part of the basisphenoid, laterally to the pituitary fossa (Figures 6 and 7). It is a thin canal that enlarges anteriorly (ø 0.6–1 mm) and has a pronounced ventral curvature (2–3 mm ventral offset), like the condition in *Osteolaemus*.

The facial nerve, or cranial nerve VII (CN VII), connects with the endocast through a small foramen in the prootic (ø 0.6–0.8 mm), posteriorly to CN V and just anteriorly to the endosseous labyrinth. It is initially short (2–3 mm long) and projected laterodorsally into the pharyngotympanic sinus (CN VII, Figures 5 and 6). At this point, it is separated into two branches that can be initially followed by their impression on the lateral side of the prootic. First, the hyomandibular branch oriented dorsally and posteriorly, is supposed to cross the pharyngotympanic sinus to join the cranioquadrate passage (see Kuzmin et al., 2021, figure 5); this branch could only be reconstructed partially in NHMUK PV R 36685. Second, the palatine branch, oriented ventrally then anteriorly, was almost entirely reconstructed (CN VII_{pal}, Figures 5–7). This canal is around 0.6 mm in diameter, and it represents the longest reconstructed nerve. It passes ventrally between CN V and the cerebral carotid arteries, before showing a 45° anterior curve ventrally to the trigeminal ganglion. The canal then proceeds ventrally, entering the basisphenoid and following a groove on the medial side of the basisphenoid recess, until they emerge on the ventral side of the braincase, near the suture between the basisphenoid and the anterodorsal part of the pterygoid. In *Voay*, the course of cranial nerve VII in the ventral part of the braincase is vertical, like in *Osteolaemus* (Figures 5 and 14a), whereas in *C. niloticus* it is horizontal (Figure 14e).

The vestibulocochlear nerve, or cranial nerve VIII (CN VIII) are short nerve branches located medially to the endosseous labyrinth, which cross the otic bulla to link the vestibular apparatus and the cochlea to the hindbrain. Two small foramina (ø 1 mm), probably corresponding to the anterior branches of CN VIII, have been reconstructed in NHMUK PV R 36684. They are located on the right side of the endocast, anteroventrally to the vestibular apparatus,

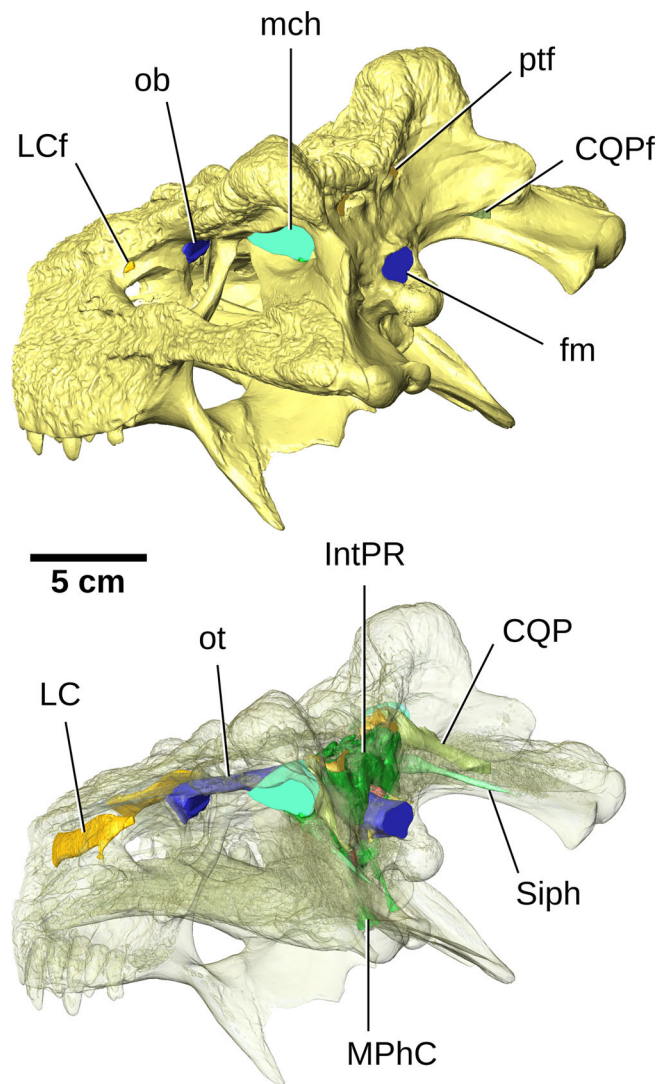


FIGURE 8 Posterior oblique view of the skull and endocranial structures showing the morphology of the lacrimal canal of *Voay robustus* NHMUK PV R 36685. Top: bones rendered opaque, showing the position of the different foramina; bottom: bones rendered transparent, showing the opaque internal cavities. CQP, cranioquadrate passage; CQPf, foramen of the cranioquadrate passage; fm, foramen magnum; IntPR, intertympanic pneumatic recess; LC, lacrimal canal; LCf, posterior foramen of the lacrimal canal; mch, meatal chamber; mpc, median pharyngeal canal; ob, olfactory bulb; ot, olfactory tract (CN I); ptf, posttemporal fenestra; siph, siphonium.

and tightly packed with the root of CN VII (Figure 6). Additionally, the ventral branch of CN VIII (the macula sacculi) could be reconstructed on the left side of NHMUK PV R 36685. It is 1.5 mm wide and 2.5 mm long and located on the suture between the prootic and the otoccipital, ventral to the otic bulla. This branch links the pons with the medial side of the cochlear duct.

The common canal for the posterior cranial nerves is the second largest neural passage of the braincase. It

contains the glossopharyngeal, vagus, and spinal accessory nerves, or cranial nerves IX–XI (CN IX–XI), and the sympathetic nerve (SN). It originates from the metotic foramen, an elongated opening on the medial surface of the otoccipital that contours the posteroventral curvature of the otic bulla. From this foramen, two canals emerge: one very thin (\varnothing 0.5 mm) and projected laterally, and one quite thick (\varnothing 2 mm) and projected posterolaterally, which probably corresponds to CN IX and CN X, respectively (Figure 6). They run through the otoccipital for 3–4 mm, before joining the course of the SN in a large passage (4 mm wide). The common canal then proceeds posterolaterally and ventrally inside the otoccipital and exits through the occipital side of the skull dorsal to the foramen of the cerebral carotid artery.

The SN follows the common canal for the posterior cranial nerve from the occipital side of the skull. Following this passage anteriorly, it separates from the cranial nerves IX–X at the level of the otic bulla to ascend dorsally, following a canal enclosed in the otoccipital, \sim 1.5 mm wide, between the *recessus scalae tympani* (RST) and the otoccipital diverticulum. Then, it follows a groove on the internal side of this same bone, which makes a laterodorsal curve and enters the posterior part of the meatal chamber to join the cranioquadrate passage (Figures 5 and 7).

The hypoglossal nerves, or cranial nerves XII (CN XII), join the brain endocast through two foramina in the otoccipital, situated along the medulla oblongata, between the metotic foramen and the foramen magnum. Two corresponding canals, the anterior and posterior branches, are projected laterally and slightly ventrally to exit the skull laterally to the foramen magnum. In *V. robustus*, the canal for the anterior branch of CN XII is two to three times thinner than the canal for the posterior branch. The anterior branch is \sim 1 mm wide and 11 mm long, while the posterior branch is 1.5–3 mm wide and 9 mm long.

4.3 | Neurovascular canals

The cranioquadrate passage is the largest neurovascular passage of the skull. It hosts the SN and the hyomandibular branch of the facial nerve (CN VII_{hyo}), as well as the stapedia and temporoorbital arteries and veins (Kuzmin et al., 2021; Porter et al., 2016). The cranioquadrate passage of *V. robustus* follows the quadrate-otoccipital suture from the posterior side of the meatal chamber to the lateroventral edge of the otoccipital. It is large but constricted anteroposteriorly (\sim 6 mm mediolateral width and \sim 3.3 mm anteroposterior width). From its posterior external foramen to the post-quadrate foramen situated

on the roof of the meatal chamber, it measures roughly 6 cm long. The position of the soft tissue suspensory plate separating the meatal chamber from the cranioquadrate passage had to be inferred from the position of two acute bony processes on the dorsal (otoccipital) and ventral (quadrate) side in the posterior part of the meatal chamber (Figures 5–8).

The temporal canal is a bony passage linking the post-temporal fenestra on the occipital side of the skull with the supratemporal fenestra anteriorly. It is linked with the cranioquadrate passage and the back of the meatal chamber through the post-quadrate foramen. It hosts the stapedia and temporoorbital arteries and veins coming from the cranioquadrate passage and irrigating the adductor muscles (Kuzmin et al., 2021; Figure 5). In adults *V. robustus*, the posttemporal fenestrae are slit-like and nearly completely closed in three out of the four studied specimens: only NHMUK PV R 36685 possesses an open posterior part of the temporal canal, which ranges from 6.5 mm in width posteriorly to 2 mm in width when entering the internal post-quadrate foramen. The post-quadrate foramen is a subcircular ostium ~7 mm in diameter, which connects the anterior part of the temporal canal to the cranioquadrate passage. The temporal canal is about 4–5 mm wide at the level of the post-quadrate foramen, and enlarges anteriorly to reach the supratemporal fenestra through the anterior temporal foramen. The anterior temporal foramina of *V. robustus* are constricted dorsoventrally and oriented medioventrally, measuring ~12.5 mm in width and ~3.4 mm in height.

The paired cerebral carotid arteries are the major blood vessels irrigating the brain endocast. Their paired canals are circular in cross section and measure ~3.3 mm in diameter, displaying a constant thickness all through their length. They penetrate the skull on the posteroventral side of the otoccipital, between its sutures with the quadrate laterally and the basioccipital medially, ventrally to the foramen of the common canal for the posterior cranial nerves. Anteromedially, they shift anteriorly under the otic bulla to enter the ventral part of the pharyngotympanic sinus, where they are enclosed in a fragile bony canal ventrally to the extracapsular buttress of the otoccipital. This bony canal is generally broken or too cartilaginous to be preserved in extant species, whereas it is thicker and well-ossified in *Voay*, allowing for the complete reconstruction of the carotid arteries through the sinus. Anteriorly to the cochlear duct, they descend anteromedially and ventrally and pass into the basisphenoid. Ventrally to the midbrain, they shift anteriorly and the left and right canals then merge in the posterior part of the pituitary fossa.

Additionally, a very thin canal (<1 mm-wide) emerges laterodorsally where the cerebral carotid artery

joins the ventral part of the extracapsular buttress. This canal is enclosed inside the extracapsular buttress and emerges at its laterodorsal tip. It hosts the arterial branch between the cerebral carotid and the stapedia arteries (ast-CC, Figures 5–7), the latter being situated in the cranioquadrate passage.

The lacrimal canal of *V. robustus* links the anterior side of the orbital cavity to the dorsal roof of the nasal cavity. The lacrimal foramen is located on the posterior face of the lacrimal, just lateral to the lacrimal-prefrontal suture, and constricted laterodorsally (~6 mm in width, 2.5 mm in length). Here, the bony wall forming the anterior margin of the orbit is high and projected posterovertrally in *V. robustus* (Figure 8). The lacrimal duct foramen is located on the medial side of the lacrimal orbital margin, thus having a lateral orientation. This condition is also found in *Osteolaemus* but not in other adult Crocodylidae representatives, whereas it is observed in juveniles. From the lacrimal foramen, the lacrimal canal enlarges lateroventrally and mediolaterally, reaching ~14 mm in width. It narrows slightly in the middle of the lacrimal (~11.6 mm wide), and enlarges again before opening in the nasal cavity, just posterior to the lacrimal-maxillary suture.

4.4 | Inner ear

The inner ear of crocodylians can be divided into the capsular portion, bounded by the otic bulla, and into the extracapsular portion, bounded by the extracapsular buttress of the basioccipital (Kuzmin et al., 2021). The endosseous labyrinths are perfectly preserved in all studied specimens, except for the ventral tip of the cochlear duct in NHMUK PV R 2204, which could not be reconstructed. The preservation of the extracapsular portion is variable and depends on the preservation of the extracapsular buttress, which may often be broken or incomplete. The most complete inner ear is found in NHMUK PV R 36684 (Figure 9).

The capsular portion of the inner ear corresponds to the endosseous labyrinth, which is located at the level of the metencephalon and encapsulated in the otic bulla. The latter is formed by the respective capsular portions of the prootic anteriorly, supraoccipital dorsally and otoccipital posteriorly, with a minor contribution of the basisphenoid to the ventral part of the lagenar recess. The dorsal component of the endosseous labyrinth is the vestibular apparatus, which is involved in equilibrium and movement perception in living animals (Bronzati et al., 2021). It is the most voluminous portion of the endosseous labyrinth, showing a sub-pyramidal shape with an average of 16.6 mm in anteroposterior length, and 12 mm in height in *V. robustus* (~57% of total height).

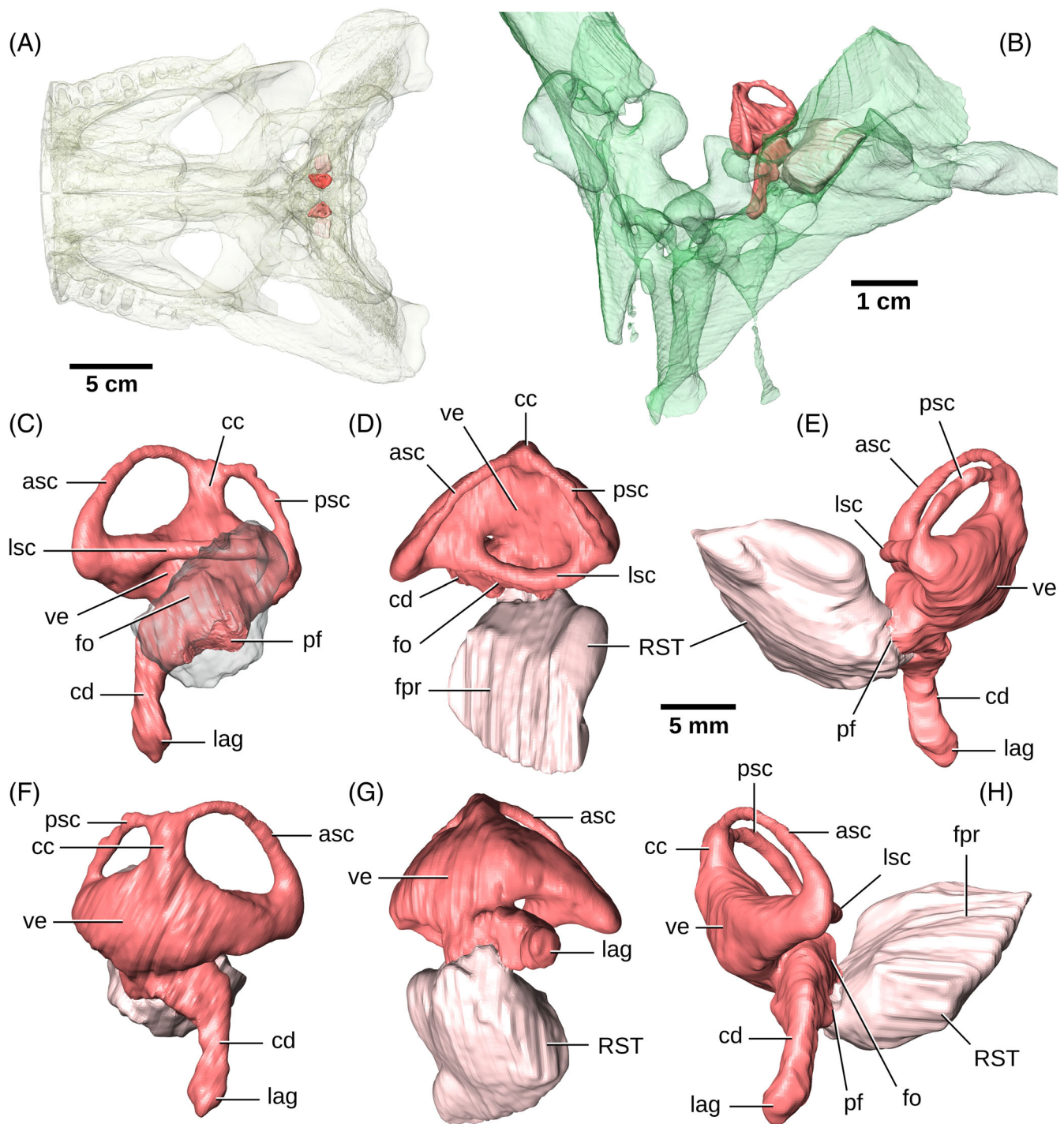


FIGURE 9 3D reconstruction of the left endosseous labyrinth and associated recesses of *Voay robustus* NHMUK PV R 36684. (a) Rear skull of NHMUK PV R 36684 in dorsal view rendered transparent, showing the position of the paired inner ears (in pink); (b) anterior oblique view of the relationship between the left inner ear (in pink) and the pharyngotympanic sinus rendered transparent (in green); (c) lateral; (d) dorsal; (e) posterior; (f) medial; (g) ventral; (h) anterior views of the left inner ear. The *recessus scalae tympani* (RST) is rendered transparent in lateral view for visualization purposes. asc, anterior semicircular canal; cc, common crus; cd, cochlear duct; fo, *fenestra ovalis* (receiving the columella); fpr, *fenestra pseudorotunda* (margins for attachment of the secondary tympanic membrane); lag, lagena; lsc, lateral semicircular canal; pf, perilymphatic foramen; psc, posterior semicircular canal; RST, *recessus scalae tympani* (hosting the perilymphatic sac); ve, vestibular recess.

The vestibule forms the base of the vestibular apparatus (ve, Figure 9). The common crus emerges dorsally to connect the anterior and posterior semicircular canals

inside the capsular portion of the supraoccipital. It is 3.2 mm in height, and is widest at its base (3.3 mm) narrowing dorsally (2.2 mm). The ampulla of the lateral

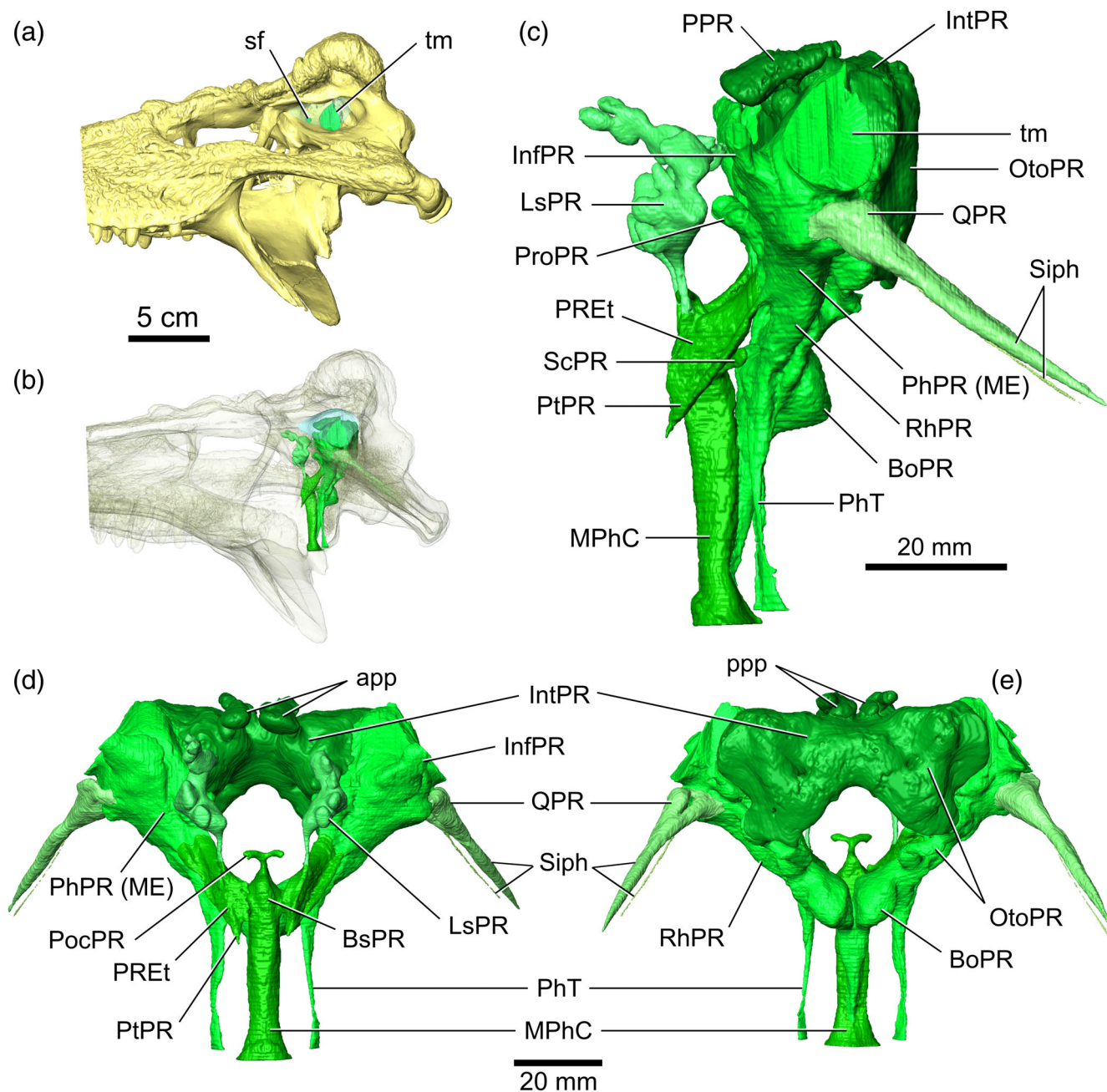


FIGURE 10 Paratympenic sinus system of *Voay robustus* NHMUK PV R 36685. (a) 3D views of the rear part of the skull showing the opening of the sinuses (in green), with the meatal chamber rendered transparent (in blue); (b) 3D view of the skull rendered transparent, showing the position of the paratympenic sinuses. 3D reconstructions of the paratympenic sinuses in (c), left lateral; (d) anterior; (e) posterior views. app, anterior processes of the parietal recess; BoPR, basioccipital pneumatic recess; BsPR, basisphenoid pneumatic recess; InfPR, infundibular pneumatic recess; IntPR, intertympanic pneumatic recess; LsPR, Laterosphenoid pneumatic recess; MPhC, median pharyngeal canal; OtoPR, otoccipital pneumatic recess; PhPR (ME), pharyngotympanic pneumatic recess (middle ear); PhT, pharyngotympanic tubes; PocPR, postcarotid pneumatic recess; ppp, posterior processes of the parietal recess; PPR, parietal pneumatic recess; PREt, pneumatic recessus epitubaricus; ProPR, prootic facial recess; PtPR, pterygoid pneumatic recess; QPR, quadrate pneumatic recess; RhPR, rhomboidal pneumatic recess; ScPR, subcarotid pneumatic recess; Siph, siphonium; sf, subtympanic foramen; tm, tympanic membrane.

semicircular canal is slightly visible as a swelling of the anterior part of the vestibule (Figure 9c). The three semicircular canals are circular in cross section; the anterior

and posterior canals are thin and sub-equal in diameter ($\varnothing \sim 0.7$ mm) while the lateral canal is twice thicker ($\varnothing 1.4$ mm). The anterior semicircular canal is higher than

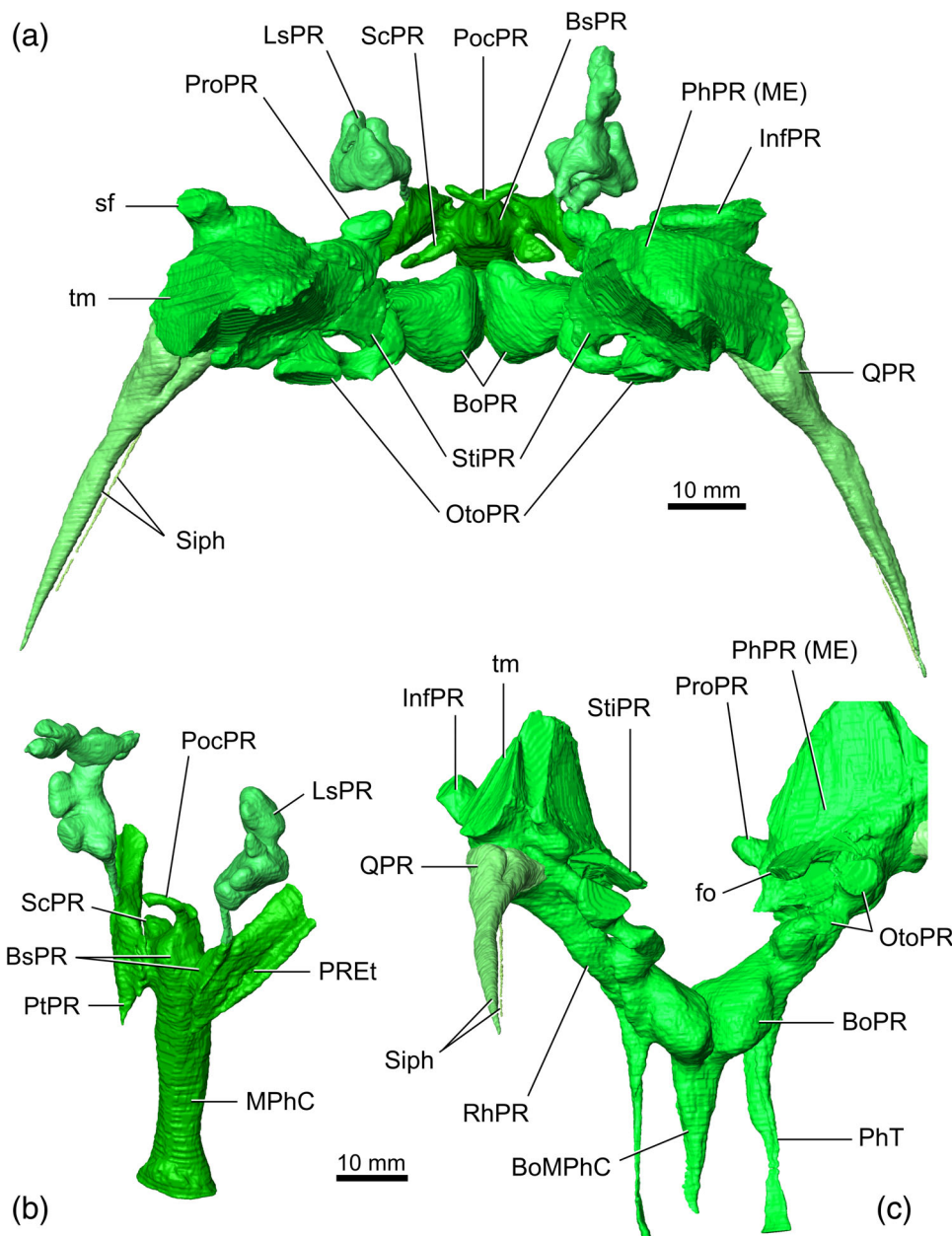


FIGURE 11 Median pharyngeal and pharyngotympanic sinuses of *Voay robustus* NHMUK PV R 36685. Paratympenic sinus system in dorsal view (a), anterior oblique view of the anterior recesses (b) and posterior oblique view of the posterior recesses (c), with the intertympanic sinus system removed. app, anterior processes of the parietal recess; BoMPhC, basioccipital portion of median pharyngeal canal; BoPR, basioccipital pneumatic recess; BsPR, basisphenoid pneumatic recess; fo, *fenestra ovalis*; InfPR, infundibular pneumatic recess; LsPR, laterosphenoid pneumatic recess; MPhC, median pharyngeal canal; OtoPR, otoccipital pneumatic recess; PhPR (ME), pharyngotympanic pneumatic recess (middle ear); PhT, pharyngotympanic tubes; PocPR, postcarotid pneumatic recess; ppp, posterior processes of the parietal recess; PPR, parietal pneumatic recess; PREt, pneumatic *recessus epitubaricus*; ProPR, prootic facial recess; PtPR, pterygoid pneumatic recess; QPR, quadrate pneumatic recess; RhPR, rhomboidal pneumatic recess; ScPR, subcarotid pneumatic recess; Siph, siphonium; sf, subtympanic foramen; StiPR, stipedial pneumatic recess communicating with the *fenestra ovalis*; tm, tympanic membrane.

the posterior one, a condition observed in the three extant crocodylid genera (~ 1.1 mm dorsal offset, Figure 9c,e,f,h). It has a large dorsomedial curve through the prootic and the supraoccipital, then turns ventrally to meet the dorsal tip of the common crus. The posterior semicircular canal is shorter and lower than the anterior one: it is three times smaller than the anterior semicircular canal area (Figure 9c). The posterior canal shows a small dorsomedial curve in the otoccipital with no dorsal offset inside the supraoccipital: it does not exceed the common crus dorsally. The lateral semicircular canal is straight, passing through the prootic anteriorly and the otoccipital ventrally; it has a pronounced lateral curve (~ 1.7 mm of lateral offset). Its size is equivalent to that of the posterior semicircular canal.

Ventrally to the lateral semicircular canal and dorsally to the cochlear duct, the vestibule shows a ventrolateral bulge, flattened laterally, which connects to the *fenestra ovalis*. The *fenestra ovalis* is the contact point for the columella. In *V. robustus* it is ellipsoidal in shape, has a mean height of 3.2 mm, and 6.2 mm in anteroposterior length. The *fenestra ovalis* communicates with the stipedial diverticulum of the middle ear (StiPR, Figure 11a,c; Tahara & Larsson, 2022). The perilymphatic foramen lies posteroventrally to the *fenestra ovalis*; it links the endosseous labyrinth to the extracapsular portion of the perilymphatic sac (Kuzmin et al., 2021). This second ostium is smaller than the *fenestra ovalis* but has a more circular shape (~ 3.5 mm in height and 4.8 mm in length; Figure 9c).

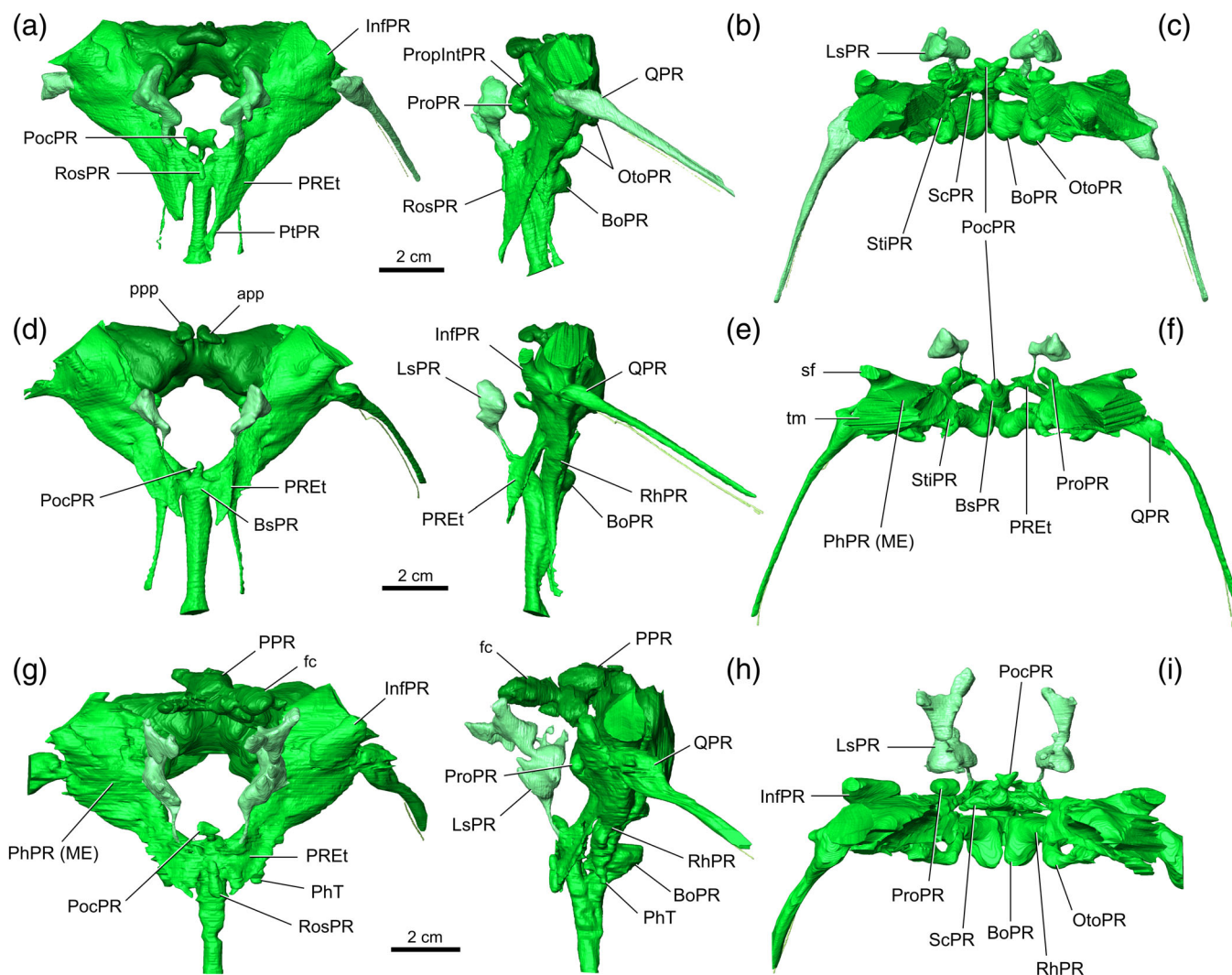


FIGURE 12 Variability of the paratympenic sinus system in other specimens of *Voay robustus*. (a–c) 3D reconstruction of the paratympenic sinuses of NHMUK PV R 36684 in anterior, left lateral, and dorsal views. (d–f) 3D reconstruction of the paratympenic sinuses of NHMUK PV R 2204 in anterior, left lateral, and dorsal views. (g–i) 3D reconstruction of the paratympenic sinuses of MHNH F 1908.5A in anterior, left lateral, and dorsal views. Intertympanic sinus system was removed in (c, f, i) for visualization purposes. app, anterior processes of the parietal recess; BoPR, basioccipital pneumatic recess; BsPR, basisphenoid pneumatic recess; InfPR, infundibular pneumatic recess; fc, frontal cavities; LsPR, Laterosphenoid pneumatic recess; OtoPR, otoccipital pneumatic recess; PhPR (ME), pharyngotympanic pneumatic recess (middle ear); PhT, pharyngotympanic tubes; PocPR, postcarotid pneumatic recess; ppp, posterior processes of the parietal recess; PPR, parietal pneumatic recess; PREt, pneumatic recessus epitubaricus; PropIntPR, prootic part of the intertympanic recess; ProPR, prootic facial recess; PtPR, pterygoid pneumatic recess; QPR, quadrate pneumatic recess; RosPR, rostral pneumatic recess; RhPR, rhomboidal pneumatic recess; ScPR, subcarotid pneumatic recess; sf, subtympanic foramen; StiPR, stipodial pneumatic recess communicating with the *fenestra ovalis*; tm, tympanic membrane.

The ventral component of the endosseous labyrinth is the cochlear duct, which hosts the basilar papilla and is involved in the auditory function in living animals (Walsh et al., 2009). It is positioned lateroventrally to the vestibule, and has a tubular shape that extends ventrally, tapering slightly in its middle. The cochlear duct is bounded medially by the medioventral part of the prootic. In *V. robustus*, the cochlear duct is straight, and almost as high as the vestibular apparatus, with 11.3 mm

in mean height (~53% of total labyrinth height). Its ventralmost part shows a posterior swelling which corresponds to a small depression in the cochlear recess, the lagenar recess, supported ventrally by the basisphenoid. This part hosts the lagena, the ventralmost part of the basilar papilla.

The extracapsular portion of the inner ear corresponds to the perilymphatic sac. It is situated laterally to the endosseous labyrinth, inside the RST (Figure 9), and

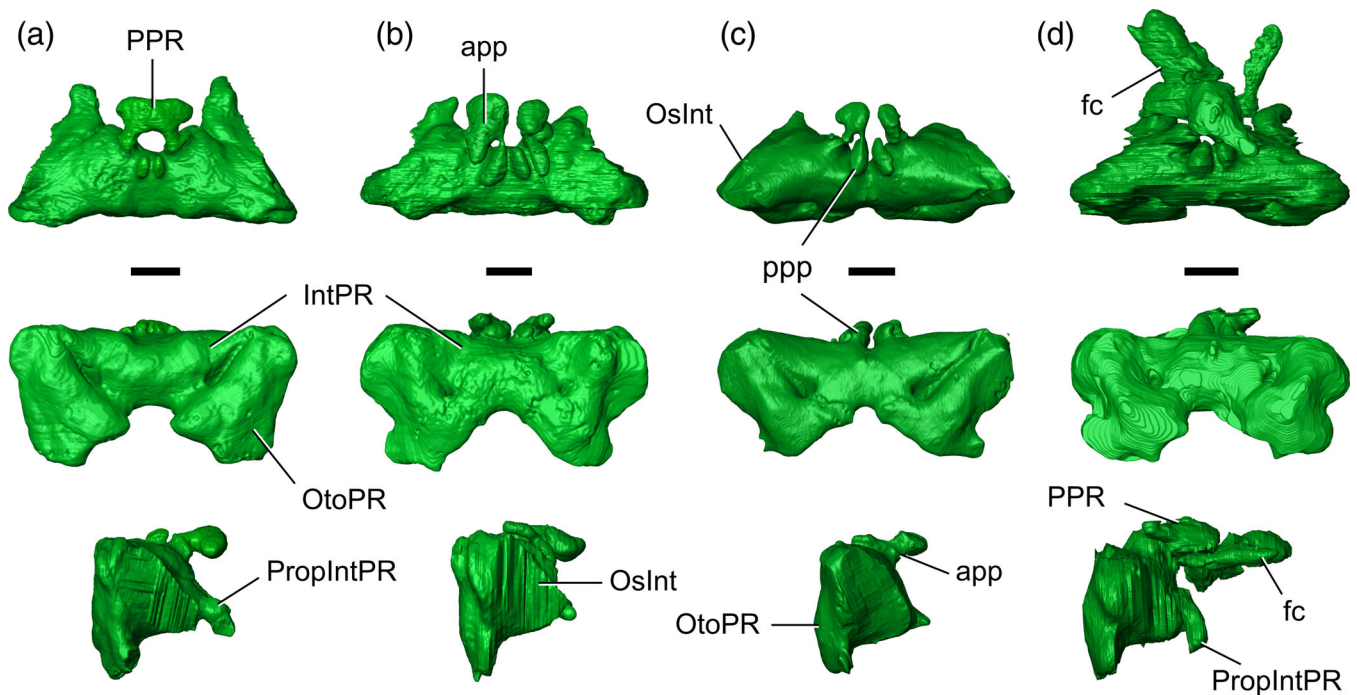


FIGURE 13 Variability of the intertympanic sinus system in *Voay robustus*. (a) NHMUK PV R 36684; (b) NHMUK PV R 36685; (c) NHMUK PV R 2204; (d) MNHN F 1908.5A in dorsal (top), posterior (middle), and right lateral (bottom) views. app, anterior processes of the parietal recess; fc, frontal cavities; IntPR, intertympanic pneumatic recess; OtoPR, otocipital pneumatic recess; ppp, posterior processes of the parietal recess; PPR, parietal pneumatic recess; PropIntPR, prootic part of the intertympanic recess.

connects to it through the perilymphatic foramen. It is a large cavity bounded posteriorly, ventrally and anterovertrally by the extracapsular buttress of the otocipital. It is preserved in its entirety in NHMUK PV R 36684. It is ~ 10.5 mm in anteroposterior length and 13.6 mm in mediolateral width. It is ellipsoidal in shape and oriented laterodorsally, with a marked ventral curvature (Figure 9e). Dorsally, it is bounded by the *fenestra pseudorotunda*, the ostium where the secondary tympanic membrane is attached in living animals (Figure 9d). The *fenestra pseudorotunda* separates the extracapsular portion of the inner ear from the pharyngotympanic sinus (Figure 9b). In *V. robustus* the *fenestra pseudorotunda* is oriented posterolaterally to medioventrally, and is ~ 11 mm long and 7.3 mm wide.

4.5 | Paratympanic sinus system

Voay robustus shows a pneumatised braincase, with a more extensive pneumatisation and larger cavities and canals (Figures 4 and 10–13). All bones of the braincase are filled by the paratympanic pneumatic recesses, including the laterosphenoids, basisphenoid, basioccipital, prootics, otocipitals, supraoccipital, and parietal, and to a lesser extent the pterygoids and the frontal (Figure 12). All these sinus

expansions are confluent. However, to ease the comparisons, we will divide the description in three parts, which correspond to three expansions of the paratympanic sinus system: the median pharyngeal sinus (Figure 11b), the pharyngotympanic sinus (Figure 11c), and the intertympanic sinus (Figure 13).

The median pharyngeal sinus invades the basisphenoid, and is composed of the median pharyngeal canal and the basisphenoid recesses (Figure 11b). The median pharyngeal canal of *V. robustus* is thick, sub-circular in cross-section and of approximately even diameter from its external foramen to the pharyngeal intersection, with a slight narrowing dorsal to the foramen (Figure 10c–e). It is of constant thickness and does not taper dorsally before entering the basisphenoid recess like it can be observed in *Osteolaemus*, *Mecistops*, or *C. niloticus* (Figure 14). The median pharyngeal canal also has a basioccipital component (posterior branch of the median pharyngeal canal sensu Colbert, 1946), corresponding to the unpaired ventral part of the basioccipital recess (Kuzmin et al., 2021). This posterior branch is slightly compressed anteroposteriorly but is nearly as voluminous as the anterior component, or even wider in NHMUK PV R 36684 (Figure 12b).

In its dorsal part, the anterior and posterior components of the median pharyngeal canal separate clearly,

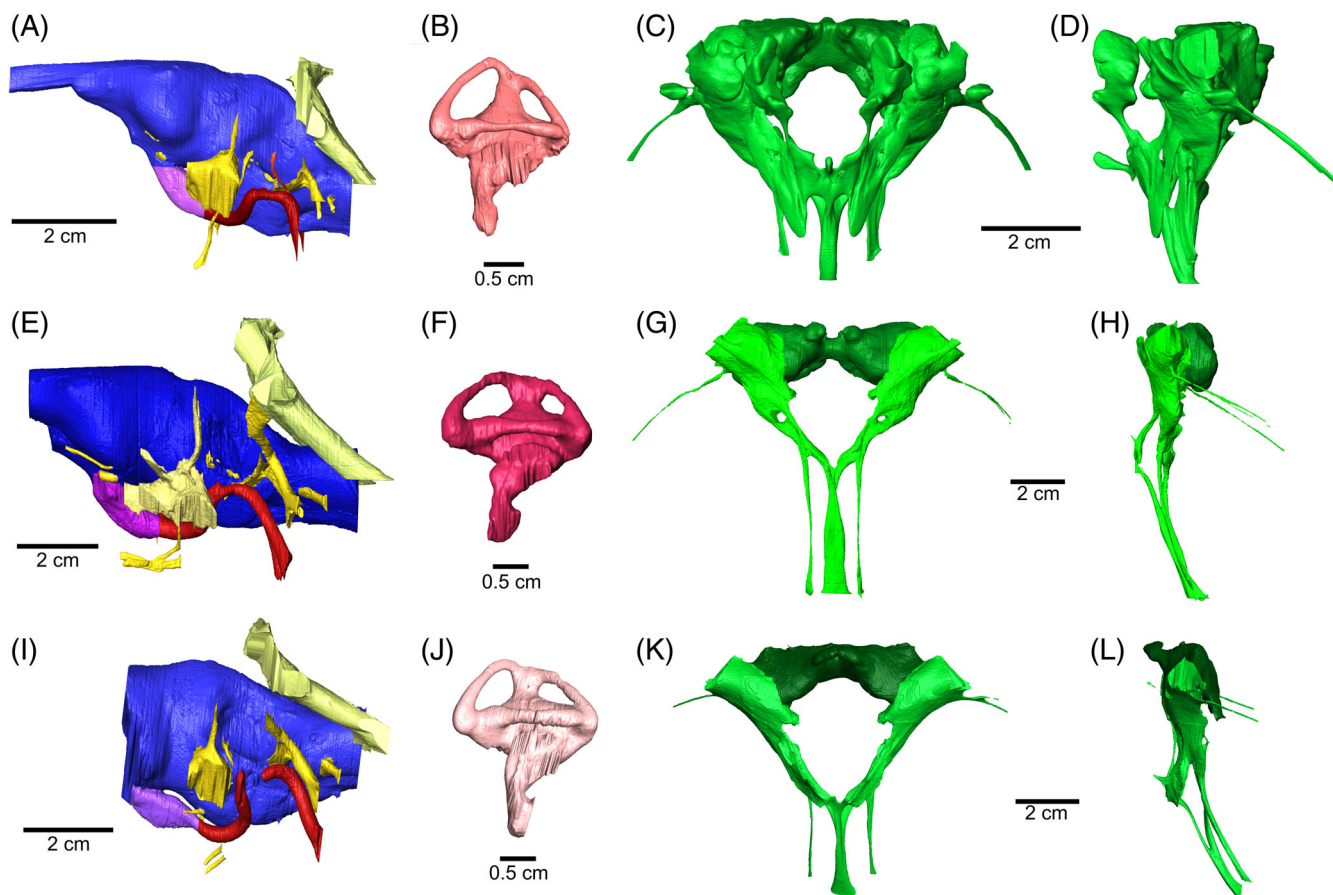


FIGURE 14 Endocranial anatomy and pneumaticity of *Osteolaemus tetraspis*, *Crocodylus niloticus* and *Mecistops* sp. used as comparative material. (a–d) *Osteolaemus tetraspis* UCBLZ 2019–1-236; (e–h) *Crocodylus niloticus* MHNL 50001387; (i–l) *Mecistops* sp. UM N89. (a, e, i) Left lateral view of the neurovascular system (blue: brain endocast; purple: pituitary fossa; red: carotid arteries; yellow: cranial nerves). (b, f, j) Endosseous labyrinth; (c, g, k) paratympenic sinus in anterior view; (d, h, l) paratympenic sinus in left lateral view (light green: pharyngotympanic sinus; dark green: intertympanic sinus).

between the anterior branch of the median pharyngeal canal forming the basisphenoid recess, and the posterior branch of the median pharyngeal canal forming the basioccipital recess. Here, this confluence is designated as the “pharyngeal intersection.” In *V. robustus*, the pharyngeal intersection shows a V-shape in lateral view, like in other extant Crocodylidae species.

The basisphenoid recess *sensu stricto* inflates the medial part of the basisphenoid. It is bulbous, and connected to the other basisphenoid recesses: the rostral, subcarotid and post-carotid recesses. The rostral recess of *V. robustus* is located anteriorly to the basisphenoid recess, and connects to the latter through the medial side of the *recessus epitubaricus*. It has a unique cylindrical shape, oriented dorsoventrally (Figures 12a,g). This recess is only present in NHMUK PV R 36684 and MHNL F 1908.5A. The subcarotid recesses are paired pneumatic cavities that open posterolaterally to the basisphenoid recess, ventrally to the cerebral carotid arteries (Figures 11a,b and 12c,i). These recesses are present in all

but one specimen of *Voay* (NHMUK PV R 2204), and only in *Osteolaemus* among extant Crocodylidae. Contrary to all adult specimens in extant Crocodylia (Kuzmin et al., 2021), *Voay* possesses a post-carotid recess, which has a variable size but is present in all specimens. The postcarotid recess of *V. robustus* is unpaired, and connected to a dorsal outgrowth of the basisphenoid recess (Figures 10d, 11a,b, and 12a,d,g). It is tubular after exiting the basisphenoid recess, and inflates the dorsal part of the basisphenoid dorsally to the carotid arteries with a pair of small lateral outgrowths. These paired outgrowths of the postcarotid recess connect with the laterodorsal part of the *recessus epitubaricus* in NHMUK PV R 36684 (Figure 12a).

The pharyngotympanic sinus of *V. robustus* has a relative volume, shape, and arrangement comparable to *Osteolaemus* (Figure 14c,d) with overall thicker diverticula, especially the basioccipital, quadrate, and middle ear recesses. The basioccipital recess consists in large sub-spherical paired cavities, 1.5–2 times wider than the

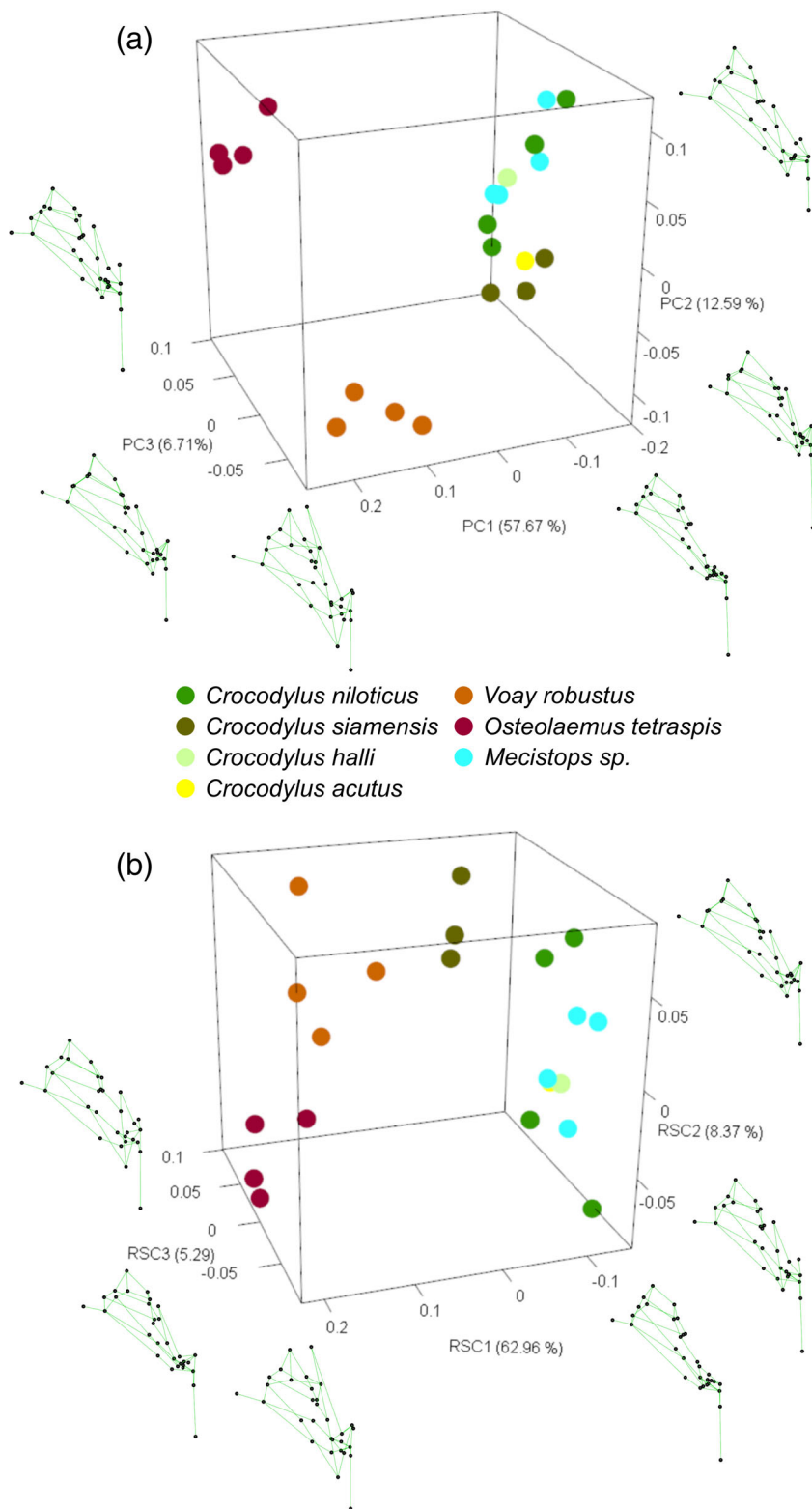


FIGURE 15 Morphospaces of the pharyngotympanic sinus shape of Crocodylidae with and without the component of size. (a) Simple PCA; (b) PCA on the residual shape coordinates after removing the common allometric component (i.e., the component of shape most correlated with size). Green wireframes correspond to extreme shapes on PC axes, showing the right pharyngotympanic sinus in anterior view.

median pharyngeal canal (BoPR; Figures 10c,e and 11a,c). It is coalescent with the rhomboidal recess latero-dorsally through the basioccipital-otoccipital suture. The rhomboidal recess inflates the braincase ventrally and laterally to the cerebral carotid artery, and is bounded by the basioccipital ventrally, by the extracapsular buttress

of the otoccipital dorsally, and by the alar process of the basisphenoid (RhPR; Figures 10 and 11). In *V. robustus*, it is anteroposteriorly thick (6–9 mm), but constricted dorsoventrally. It connects with the basioccipital recess medioventrally, with the pharyngotympanic tubes ventrally, with the middle ear recess dorsally, and with the ventral

portion of the otoccipital recess posteriorly. The pharyngotympanic tubes connect the ventral part of the rhomboidal recess to the pharynx (PhT, Figures 10 and 11c). They pass between the basisphenoid and the basioccipital, and exit the braincase through the pharyngotympanic foramina. The tubes are constricted mediolaterally, measuring around 29 mm in height, and 1 to 3.6 mm in width, but they are often partly filled, which makes difficult their reconstruction depending on the specimen. The pharyngotympanic foramina are slit-like and located laterally and slightly posterodorsally to the median pharyngeal foramen.

Anteriorly to the cerebral carotid arteries lies the pneumatic *recessus epitubaricus*, which inflates the lateral surface of the basisphenoid and the medial surface of the pterygoid and prootic. It is large dorsoventrally and mediolaterally, and compressed anteroposteriorly, like an air-filled triangular-shaped lamina (PREt; Figures 10 and 11). It connects the basisphenoid recess medially to the middle ear cavity laterodorsally. Ventrally, it narrows when entering the main body of the pterygoid to form the pterygoid recess, which is only slightly inflated in *V. robustus*: it is not well-developed ventral to the suture except in one specimen (NHMUK PV R 36684, see Figure 12a).

V. robustus possesses a laterosphenoid recess, a feature that is only shared with *Osteolaemus* among other extant Crocodylidae (Figure 14c,d). It is connected to the dorsomedial part of the *recessus epitubaricus* through a subcircular canal of variable width (0.5–3 mm), crossing the suture with the basisphenoid. The laterosphenoid recess of *V. robustus* is well developed dorsally, and reaches the level of the tympanic membrane (LsPR; Figures 10 and 12). It shows a pronounced crescent-shape in frontal view and bears a few bulbous pneumatic processes inflating the laterosphenoid slightly anteriorly. In two specimens (MHNN F 1908.5A and NHMUK PV R 36685), it bears a secondary pneumatic recess connected anterodorsally and oriented anteriorly, which inflates the dorsal part of the laterosphenoids, surrounding the endocast of the cerebral hemispheres (Figures 11b and 12h,i). This condition is variable among the studied specimens, but is unique among extant Crocodylia species studied.

The pharyngotympanic recess *sensu stricto*, or middle ear cavity, is the central body and most voluminous part of the pharyngotympanic sinus system. It links the tympanic membrane to the inner ear, and hosts the collumela. This pneumatic space is well developed ventrally and laterally in *Voay*. It is connected to the rhomboidal recess ventrally, the *recessus epitubaricus* anteroventrally, the prootic facial recess anteriorly, the infundibular recess anterolaterally, the quadrate recess laterally, the otoccipital recess posteriorly, and the intertympanic recess dorsomedially. The middle ear cavity tapers

towards the inner ear; dorsally to the extracapsular buttress, it is compressed dorsoventrally, forming the stapedial recess that surrounds the collumela and connects with the endosseous labyrinth through the *fenestra ovalis* (Figure 11c). The stapedial recess is separated from the RST by the *fenestra pseudorotunda* and the *crista interfenestralis* of the otoccipital (fig. 13 in Kuzmin et al., 2021).

All the secondary recesses aforementioned and connected to the pharyngotympanic cavity are similar in relative size and arrangements to the condition found in *Osteolaemus* (Figure 14c,d). *V. robustus* displays a bulbous prootic facial recess, variably connected to the prootic part of the intertympanic diverticulum dorsally in two out of the four specimens studied (Figure 12b,h). The ventral portion of its otoccipital recess is also bulbous in shape and surrounds the posterior portion of the cerebral carotid arteries laterally. The infundibular recess is flattened anteroposteriorly and developed mediolaterally and dorsoventrally, largely inflating the anterior part of the quadrate. In contrast, in *C. niloticus*, this recess is only a canal sub-circular in cross-section (Figure 14). The infundibular and quadrate recesses are connected anteroposteriorly through a small ostium ventral to the meatal chamber, except in NHMUK PV R 36685. The quadrate recess is especially voluminous in *Voay*: it consists of a bulla elongated posterolaterally, located lateroventrally to the tympanic membrane and largely connected to the pharyngotympanic cavity. Its posterior side tapers laterally and becomes the siphonium, which connects the quadrate recess to the articular recess. This condition is slightly different from *Osteolaemus*, where the quadrate recess is developed more laterally and anteriorly and is clearly separated by small ostia from both the pharyngotympanic recess and siphonium (Figure 14c,d). The siphonium of *Voay* is thus coalescent with the posterior part of the quadrate recess, and it is relatively larger than in any other studied Crocodylidae (~3.8 mm in starting width). It then tapers gradually toward the articular. The siphonium exits the skull through the foramen aereum (<2 mm in diameter), located on the medial side of the quadrate. The siphonium is doubled by an extremely thin canal that follows its course ventrally.

The intertympanic sinus system of *V. robustus* displays an expanded pneumatization and is largely confluent with the pharyngotympanic sinus. Its diverticula link the left and right pharyngotympanic cavities above the hindbrain (Figures 4 and 13, see also Perrichon, Hautier et al., 2023). The prootic buttress surrounds the ostium between the intertympanic recess and the middle ear cavity. The intertympanic recess is anteroposteriorly and dorsoventrally expanded, contrary to the condition of *C. niloticus* where it prominently narrows dorsoventrally in its medial part (see fig. 5 in Perrichon, Hautier et al., 2023). Its prootic

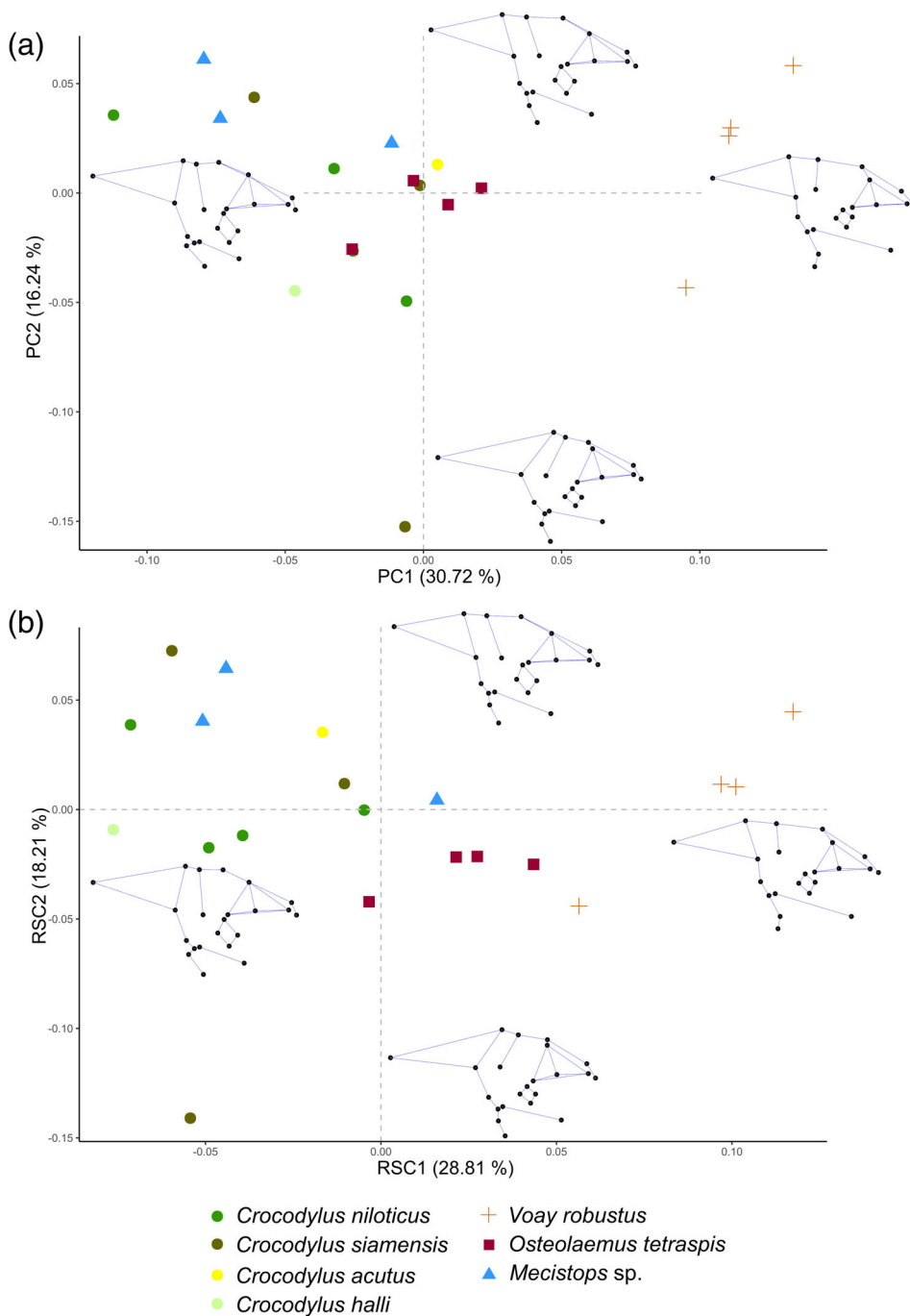


FIGURE 16 Morphospaces of the brain endocast shape of Crocodylidae with and without the component of size. (a) Simple PCA; (b) PCA on the residual shape coordinates after removing the common allometric component (i.e., the component of shape most correlated with size). Blue wireframes correspond to extreme shapes on PC axes, showing the left side of the brain endocast in left lateral view.

part is developed anteriorly; it is variably connected to the prootic facial recess like in *Osteolaemus*. The otoccipital recess is voluminous and well-developed ventrally; it is connected to the rhomboidal recess ventrally and to the pharyngotympanic recess lateroventrally through large ostia. The parietal is inflated by the four preparietal processes, which variably form a single parietal recess. The anterolateral preparietal processes are directed anteriorly and merged in a single cavity in MNHN F.1908.5A and NHMUK PV R 36684. The posteromedial preparietal processes are directed vertically and are slightly expanded

anteroposteriorly, variably connected anteriorly to the anterolateral processes (Figure 13b–d). The individual development of the parietal recess seems to differ depending on the specimen studied. It is greatly inflated in MNHN F 1908.5A, and carves a large pneumatic cavity oriented anteriorly that inflates into the frontal (frontal cavity, Figures 12g,h and 13d). In the other specimens, the parietal recess is smaller; the anterolateral pre-parietal processes are also slightly developed in the posterior direction in NHMUK PV R 36685, like in some specimens of *Osteolaemus* (Perrichon, Hautier et al., 2023).

5 | SHAPE ANALYSES

5.1 | Morphometry of the pharyngotympanic sinus

The shape of the pharyngotympanic sinus is significantly correlated to the species-specific morphology as the major variable ($R^2 = 68.4\%$, $p = 0.001$), as well as to the size of the specimens as a minor variable ($R^2 = 13.3\%$, $p = 0.001$). Based on Procrustes distances, *Osteolaemus* and *Voay* as a group can always be statistically distinguished from other extant Crocodylinae (p -values < 0.05). *Crocodylus* and *Mecistops* cannot be significantly separated, nor *Voay* and *Osteolaemus* can be distinguished from one another (outputs of the Procrustes ANOVAs and pairwise comparisons are available in Data S1).

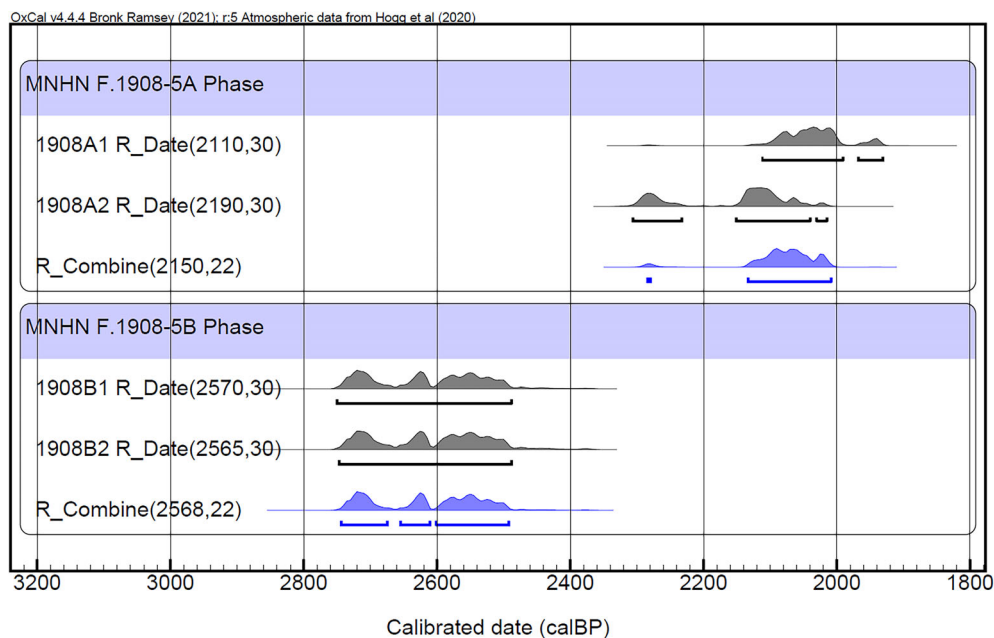
The first analysis performed was a simple PCA of the Procrustes coordinates. The first three principal components (PC) explain 76.97% of the total variance contained in our dataset, and shows a clear morphological gap between *Voay*, *Osteolaemus* and Crocodylinae, as well as between *Voay* and *Osteolaemus*, which are both clearly separated in shape space (Figure 15a). PC1 explains 57.7% of the total variance, and reflects the visible morphological differentiation observed between Crocodylinae and the two osteolaemine genera (axis values being correlated to species groups, $R^2 = 92.5\%$, $p = 0.001$). This axis represents changes in the expansion of all pneumatic diverticula. The positive values correspond to greatly inflated basioccipital, basisphenoid, laterosphenoids, prootic, and infundibular recesses as well as a large *recessus epitubaricus*, where the *Osteolaemus* and *Voay* clusters are located. PC2 explains 12.6% of the total variance, and mainly captures changes in the size of the median

pharyngeal canal, which separates *Voay* from *Osteolaemus* in space shape (the latter having a shorter canal), but this feature is primarily correlated to size ($R^2 = 84.2\%$, $p = 0.001$). However, *Osteolaemus* also forms a distinct cluster along PC3, which is only correlated to species groups ($R^2 = 89.4\%$, $p = 0.001$). PC3 explains 6.71% of the total variance, and corresponds to changes in the orientation of the median pharyngeal canal and the posterior growth of the basioccipital recess, with *Osteolaemus* clustered in the positive values, corresponding to a median canal oriented more posteriorly and a basioccipital recess less inflated posteriorly.

In this morphospace, *Voay* is isolated as a distinct cluster in shape space, showing inflated diverticula, a posterior growth of the basioccipital recess, and a longer and more vertically oriented median pharyngeal canal. It is located far away from the small cluster of *Osteolaemus* and from the larger grouping of *Crocodylus* and *Mecistops* specimen, the latter confined in PC1 negative values. *Mecistops* and *Crocodylus* species cannot be separated; only *C. siamensis* specimens seem to be distributed along the margin of this cluster, toward PC1 more positive values.

As size still plays a role in the shape distribution of the first morphospace (explaining 4.2% of PC1 values and 84.2% of PC2 values), a second PCA was performed on the residual shape coordinates left after removing the CAC of shape (regression of shape on size). The resulting PCs are the RSC, forming a morphospace independent of size (Figure 15b). The morphospace of the first three RSCs explains 76.62% of the total variance, thus without allometry. Most of the variance is now concentrated in RSC1 (63%), which is equivalent to PC1 of the previous complete morphospace ($R^2 = 96.4\%$, $p = 0.001$). It represents the joint expansion of all diverticula, and reflects even more strongly

FIGURE 17 Calibrated dates in cal BP obtained for MNHN F.1908.5A (*Voay robustus*) and MNHN F.1908.5B (*Crocodylus* sp.). Dates calculated for the two duplicates are displayed in gray, and the combined dates are displayed in blue.



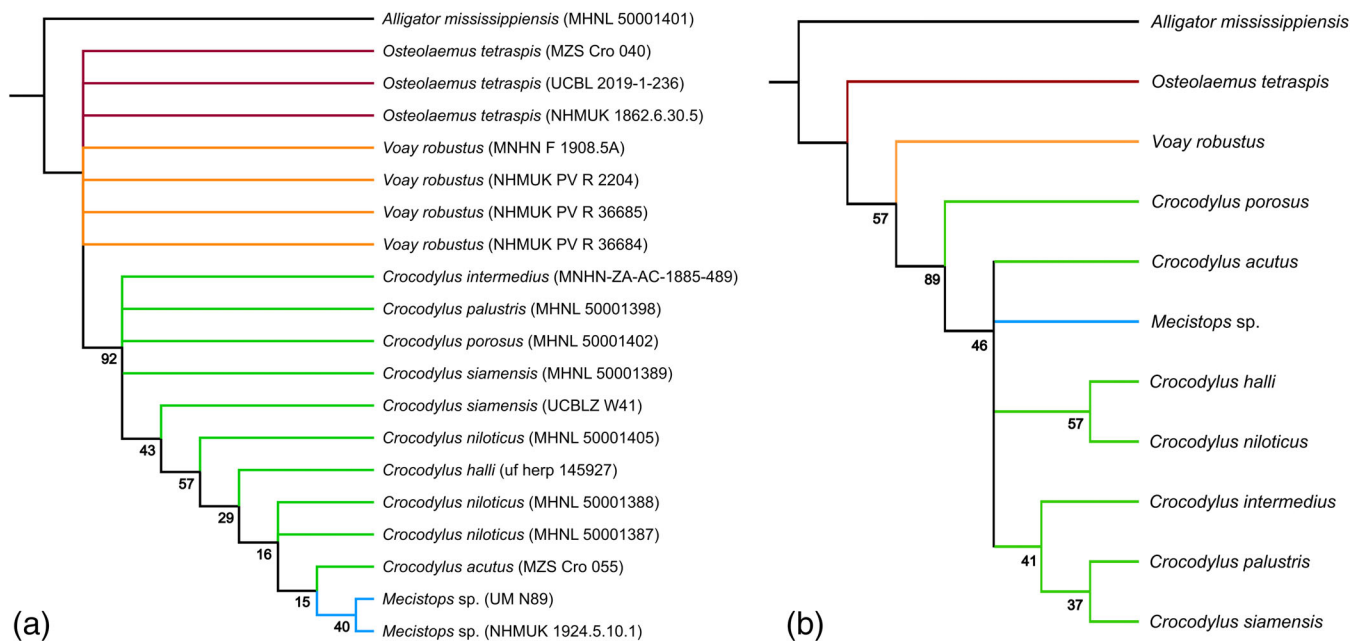


FIGURE 18 Consensus of maximum parsimony cladistic analyses for Crocodylidae including *Voay robustus*, using an endocranial-only character matrix. (a) Topology retrieved using the preliminary set of internal characters and specimens as operating taxa; (b) topology retrieved using the final set of selected internal characters and species as operational taxonomic units. *Osteolaemus* = dark red; *Voay* = orange; *Crocodylus* = green; *Mecistops* = blue. Node values corresponds to bootstraps scores.

its correlation with species class ($R^2 = 96.8\%$, $p = 0.001$). RSC2 values explains 8.37% of the allometry-free variance and are also strongly correlated to species-specific morphology ($R^2 = 92.5\%$, $p = 0.001$). This component is equivalent to PC3 of the previous complete morphospace ($R^2 = 97.8\%$, 0.001), showing a ventral orientation of the median pharyngeal canal and a posterior inflation of the basioccipital recess in positive values (Figure 15b). The third component, RSC3 is correlated to species and explains 5.29% of the total variance. Its values are linked to the relative expansion between the laterosphenoid recess and the pterygoid recess, and to the ventral expansion of the rhomboidal recess: negative values are linked to a reduced pterygoid recess and a ventrally flattened rhomboidal recess, whereas positive values are linked to a developed pterygoid recess and an inflated rhomboidal recess. This axis further discriminates the previous crocodyline cluster: *C. siamensis* specimens are isolated from other *Crocodylus* species and *Mecistops* towards RSC3 positive values. In this size-free morphospace, *Voay* and *Osteolaemus* can only be separated based on RSC2 values.

5.2 | Morphometry on the brain endocast

Overall, the shape of the brain endocast in the subset Crocodylidae does not seem to hold much information,

but still confirms that *Voay* possesses a distinguishable brain shape (Figure 16). The Procrustes ANOVA of the Procrustes coordinates shows a significant correlation of size and species on total shape, explaining, respectively, 10% ($p = 0.005$) and 45.3% ($p = 0.001$) of the variance. Pairwise comparisons between genera show that *Voay* can be significantly distinguished from all other extant crocodylids based on endocast shape, but the other genera cannot be separated from each other.

The PC analyses performed on the total and allometry-free shapes revealed equivalent results. Only the first component PC1 shows a significant relationship with species class ($R^2 = 0.76$, $p = 0.003$). It explains 30.7% of the total variance and discriminates *Voay* from other crocodylids clustered in negative values (Figure 16a). Positive values on this axis correspond to a vertically oriented pituitary fossa, an anteroposteriorly longer midbrain, and smaller otic bulla and trigeminal ostium. PC2 explains 16.2% of the total variance and corresponds to changes in the anteroposterior expansion of the cerebrum. However, PC2 is only correlated to the interaction term between species and size, showing that PC2 values are modulated by size differently in each species class, and that this parameter is rather specimen-dependent. Other axes show a seemingly random distribution of the specimens, controlled neither by size nor phylogenetic clustering.

When allometry is removed (Figure 16b), the residual components are nearly identical and the distribution of

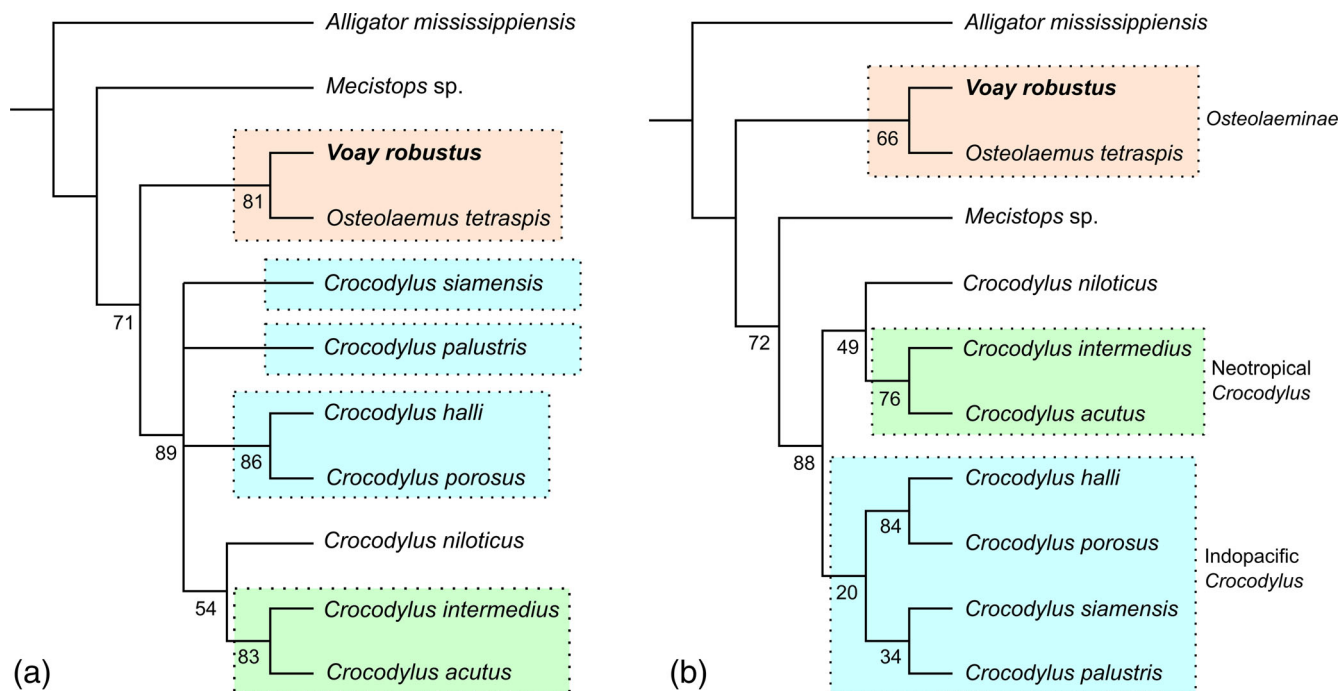


FIGURE 19 Comparison of the topologies resulting from a traditional, external-only character matrix and with the addition of selected endocranial characters, on the subset of Crocodylidae studied. (a) Result of the maximum parsimony analysis using the 195 characters matrix from (Brochu et al., 2022); (b) result of the maximum parsimony analysis using the same matrix with the addition of the 15 endocranial characters used in Figure 18b.

the specimens in space shape is similar to the previous PCA, but the clustering of *Voay* in RSC1 positive values is less clear. In this allometry-free space shape, *Osteolaemus* specimens are not overlapping anymore with the rest of Crocodylidae, but the precise morphological feature responsible for this slight shape separation could not be determined (Figure 16b).

6 | RADIOCARBON DATING

On each of the dated specimens, two measurements have been obtained. For each specimen, the two radiocarbon dates were combined using the R_Combine function in OxCal program. Radiocarbon ages and the resulting calibrated dates can be found in Table 2 and are displayed in Figure 17.

The combined radiocarbon date obtained for the *Voay* specimen MNHN F.1908.5A is 2150 ± 22 BP, corresponding to a calibrated date between 2140 and 2010 cal BP (with a 94.5% probability). In the same way, the combined radiocarbon date obtained for the *Crocodylus* specimen MNHN F.1908.5B is 2528 ± 22 BP, which corresponds to a calibrated date between 2750 and 2670 cal BP (with a 30.2% probability) or between 2660 and 2490 cal BP (with a 65.2% probability).

7 | CLADISTIC ANALYSES

The preliminary analysis of endocranial characters recovered 24 equally parsimonious trees (number of steps = 43). The strict consensus tree shows many unresolved relationships (number of steps = 56; CI = 0.554; RI = 0.725; Figure 18a). The genus *Crocodylus* is recovered as paraphyletic, with the two specimens of *Mecistops* being included and retrieved as the most derived members of a “*Crocodylus*” clade. Several specimens of the same species (i.e., *C. niloticus* and *C. siamensis*), could not be recovered as single monophyletic entities. The two American crocodiles do not cluster together: *C. intermedius* lies at the base of the genus in a polytomy with *C. palustris*, *C. porosus*, and one specimen of *C. siamensis*; whereas *C. acutus* clusters with *Mecistops* specimens in a more derived position. Finally, both *Osteolaemus* and *Voay* are recovered as paraphyletic: all specimens of the two genera are branching on a polytomy at the base of crocodylid relationships.

The second analysis recovered one maximally parsimonious tree (number of steps = 20; CI = 0.850; RI = 0.833; Figure 18b). *Osteolaemus* is recovered at the base of crocodylid relationships, whereas *Voay* is positioned as a stem-taxon to the genus *Crocodylus*. In this topology, *Crocodylus* species are again retrieved as paraphyletic, because

Mecistops is still branching among them. *C. porosus* lies at the base of the genus, in stem-position to a polytomy clustering *C. acutus*, *Mecistops* and two distinct groups: first, *C. niloticus* and *C. halli*, which share the ventral reduction of their otoccipital recess (char. 15–2); second, a group comprising *C. intermedius*, *C. palustris* and *C. siamensis*, which share an anterodorsal development of their parietal recess (char. 13–2). *C. palustris* and *C. siamensis* are retrieved together based on the incomplete reduction of their laterosphenoid recess compared to other *Crocodylus* species (char. 8–1).

Compared to *Alligator mississippiensis*, Crocodylidae is characterized by: (1) the absence of an ostium connecting the parietal and the prootic (char. 14–1; already proposed in Perrichon, Hautier et al., 2023); (2) the siphonium emerging on the posteromedial corner of the posterior quadrate ramus (char. 12–0; already mentioned in Brochu, 1997; Rio & Mannion, 2021); and (3) a V-shaped pharyngeal intersection in lateral view (char. 4–0; new). The autapomorphies of *Voay* in this analysis are: (1) the concave lateral slopes of the cerebrum (char. 1–1); (2) the dorsoventrally constant thickness of the median pharyngeal canal (char. 3–0); and (3) the presence of the postcarotid recess (char. 6–1).

When including our endocranial characters in the larger character matrix of Brochu et al., 2022, we observed a substantial change in the recovered topology. Using the original matrix, restricting the sample to the crocodylid taxa we studied, we retrieved three equally parsimonious trees (number of steps = 130). The strict consensus tree (number of steps = 131; CI = 0.824; RI = 0.610) shows *Voay* clustered with *Osteolaemus*, which is consistent with previous results. Relationships within the genus *Crocodylus* are poorly resolved: *C. niloticus* is found at the base of the Neotropical species clade, whereas the Indopacific taxa interrelationships are unresolved, branching in a polytomy at the base of the genus (Figure 19a).

After expanding this matrix with the 15 endocranial characters selected earlier, which produced the topology showed in Figure 18b, the analysis retrieved one maximally parsimonious tree (number of steps = 157; CI = 0.796; RI = 0.584), now with more resolved relationships (Figure 19b). The position of *Voay* remains unchanged, close to *Osteolaemus*, but the node is far less supported (from 81% to 66% bootstrap value). However, several new synapomorphies support a clade comprising *Mecistops* and the genus *Crocodylus* (Figure S17): the disappearance of the subcarotid, laterosphenoid and prootic recesses (char. 201–0, 202–0, and 205–0, respectively); and the lateral reduction of the otoccipital recess (char. 209–1). The interrelationships within the genus *Crocodylus* are also affected: first, the clade comprising *C. niloticus* and Neotropical *Crocodylus* species is conserved; second, and most importantly, the Indopacific

taxa are now clustered in a single resolved clade. *C. palustris* and *C. siamensis* are retrieved as sister-taxa, supported by two endocranial synapomorphies: the intermediate growth of their laterosphenoid recess (char. 202–1) and the dorsal development of their parietal recess (char. 207–2).

8 | DISCUSSION

8.1 | The internal morphology of *V. robustus* as compared with its extant relatives

Voay possesses endocranial features that can be easily distinguished from *Crocodylus*, especially concerning the paratympanic sinuses. These features are reminiscent of the internal morphology of *Osteolaemus*, but *Voay* also possesses several autapomorphic characters.

Voay shares characteristic neuroanatomical features with *Osteolaemus*. For example, the marked sigmoid outline of the brain endocast in lateral view is also found in the extant dwarf crocodile (Figure 14a). However, the sigmoid shape of the brain endocast may change during ontogeny, as it is known that the brain undergoes prominent modifications in orientation during cranial growth, both in terms of elongation and flattening (Beyrand et al., 2019; Hu et al., 2021; Watanabe et al., 2019). The similar brain endocast shapes of the two genera may relate to similarities in their cranial shapes, which are characterized by dorsoventrally high rostrum and braincase, and a less flat cranium in adult stages than in other crocodylids. The moderate “altirostry” shared by these two genera, showing a deeper lateral profile, regardless of their size, could be linked to the retention of a dorsoventrally high brain endocast. However, in absence of an ontogenetic study of this structure, considering this feature as appropriate in a taxonomic context seems premature. Additionally, the sigmoidal shape of the endocast is not involved in the shape modifications between species as captured in the PCs of the morphometric analysis (Figure 16), which shows that this feature could hardly be coded in a discrete character matrix without choosing arbitrary measurements intervals.

Among extant crocodylids, a few neuroanatomical features, however, are unique to *Voay*: the concave anterior and posterior slopes of the cerebral hemispheres, forming a spade-shape in dorsal view (Figure 5); and the peculiar squared shape, ventrally oriented pituitary fossa. Yet, the orientation of the pituitary fossa could not be coded as it was found to be highly variable intraspecifically in the other extant genera studied, often fluctuating from posterior to posteroventral. This structure was not

included in the character matrix but remains an important autapomorphy of adult *Voay*. Other features distinguishing *Voay* from extant Crocodylidae were detected in the morphometric analysis: the relatively greater mid-brain and optic region, associated with a relatively smaller otic bulla (Figure 16a); and the prominent optic lobes protruding on the laterodorsal surface of the midbrain, which is a feature that can be found, although less pronounced, on the endocast of *Osteolaemus* (Figure 14a).

Many characters of the paratympanic sinuses are also found in both *Voay* and *Osteolaemus*: first, the presence of the laterosphenoid, prootic facial, and subcarotid recesses, which are unique structures among extant adult crocodylids; secondly, the greater expansion of the basisphenoid and basioccipital recesses, as well as enlarged *recessus epitubaricus*, infundibular, quadrate, intertympanic, and otoccipital recesses. These characteristics distinguish the two genera from all other studied species of Crocodylidae, and are visible along PC1 and RSC1 axes of the total and allometry-free morphospaces (Figure 15). The differentiation in endocranial morphology between *Voay* and *C. niloticus* is thus confirmed statistically (p -value = 0.008 on the pairwise comparison between means) and can be assessed following the presence/absence of these braincase recesses, associated with the overall greater volume of the sinuses in *Voay*.

Voay and *Osteolaemus* clusters overlap on the first PC of both sinus morphospaces and cannot be statistically separated based on the pairwise comparisons of mean Procrustes shape (p -value = 0.099). They show similar pharyngotympanic sinus shapes when compared to all other crocodylids. Such inflated sinus cavities and additional diverticula are generally seen in taxa sharing a short and broad rostrum, like *Caiman* and *Paleosuchus* (Kuzmin et al., 2021). The same similarities can be observed when comparing intertympanic sinus morphologies (Perrichon, Hautier et al., 2023).

The differentiation between the two genera is visible on two other aspects of sinus shape. First, the relative length of the median pharyngeal canal is smaller in *Osteolaemus*: it is about 30% of the total sinus height, compared to about 50% in *Voay*. This variation is highly related to the specimens' sizes in our dataset, showing that size differences appear clearly on the length of the median pharyngeal canal, even between adults. Thus, despite an overall similarity in number and shape of their sinus diverticula, *Voay* possesses a more "adult-like" pharyngeal canal compared with *Osteolaemus*, the latter retaining a smaller size and a shorter median canal. However, *Voay* cannot be simply considered as a larger and older skull type version of *Osteolaemus*, because it still appears as a single cluster in the sinus morphospace

when allometry is removed: RSC2 values still separate the two genera (Figure 15b).

Then, several autapomorphies discriminate the two genera based on sinus morphology. First, the presence of an unpaired post-carotid recess, which emerges from the dorsal roof of the basisphenoid recess, is unequivocally a unique feature of *Voay*. In extant species, this recess is normally present only in embryos and hatchlings (Kuzmin et al., 2021). In *Voay*, it is present in all four adult specimens studied. It shows different degrees of development, from a small tubular protrusion (NHMUK PV R 2204) to a developed cavity that projects paired dorsal protrusions and paired ventral processes that connect back to the *recessus epitubaricus* (NHMUK PV R 36684). Additionally, the orientation of the median pharyngeal canal changes between the two genera, with a ventrally oriented canal in *Voay*, contrary to *Osteolaemus* where it is oriented more posteroventrally (captured by PC3 and RSC2 axes of the total and allometry-free morphospaces, respectively). Finally, the siphonium is coalescent with the quadrate recess and shows a large diameter, which is also a unique feature of *Voay* among crocodylids.

One of the studied specimens, NHMUK PV R 2204, is particularly interesting, as its sinuses are much less inflated (Figure 12d–f). It possesses less expanded diverticula overall, more compressed canals, and a complete absence of the subcarotid recesses. This lesser expanded morphology is reminiscent of the patterns observed in *C. niloticus*, where large adults are found to possess highly compressed sinuses (Figure 14g,h), and even obliterated eustachian canals in old individuals compared to sub-adults and juveniles. Nonetheless, this specimen still clusters with the three other *Voay* specimens in the morphospaces of the pharyngotympanic sinus. This shows that the presence of the subcarotid recesses or the large expansion of sinus cavities are not the most defining characters of *Voay*. Contrastingly, the combined presence of the laterosphenoid, prootic facial and postcarotid recesses, the ventral orientation of the median pharyngeal canal, and the posterior development of the basioccipital recess, all constitute important characters that are characteristic of *V. robustus*. This pattern of increased compression of sinuses is here only observed in NHMUK PV R 2204, which is the second largest specimen in our dataset, showing that this phenomenon is probably dependent on bone-to-sinus relative growth, and may be correlated with size (Perrichon, Hautier et al., 2023). This pattern is however variable among our sample with MNHN F.1908.5A, the largest specimen, still showing largely inflated sinuses and subcarotid recesses, and possessing additional pneumatization in the frontal and the laterosphenoids (Figure 12g–i).

These characters agree with the external cranial characters pointed out by Brochu (2007) concerning *Voay*. The endemic Malagasy crocodile indeed possesses characters that are typically seen nowadays in dwarf and small species: that is, *Osteolaemus* and *Paleosuchus*, which both possess a short and deep snout, reduced supratemporal fenestrae, and additional and inflated sinus diverticula. *Voay* shares these characteristic features (associated with additional autapomorphies) despite having a large size comparable to *Crocodylus* (at least 3 m). This shows that the common expansion of the sinuses in these extant species are not closely related to size, but rather to skull shape or ecological parameters. In *Voay*, the relative sinus volume is even slightly greater than in *Osteolaemus*. The question remains as to whether this similarity is a product of phylogenetic clustering or morphological convergence.

8.2 | Relevance of endocranial characters for the affinities of *Voay* and *Crocodylidae*

The cladistic analyses performed in this study can help to assess the phylogenetic relevance of selected endocranial characters. First, we observe that the preliminary matrix retrieves a topology that is particularly driven towards longirostry (Figure 18a): the more derived position in this first tree corresponds to specimens with an increasing ratio of rostrum length-to-width, from blunt skulls at the base (*Osteolaemus*, *Voay*, *C. palustris*) to slender skulls at the top (*C. acutus*, *Mecistops*). Specimens with “intermediate” skull shapes (*C. porosus*, *C. siamensis*, *C. niloticus*, and *C. halli*) are scattered between the two extremes. The specimen of *C. intermedius* is an exception, as its skull morphology is close to *C. acutus*, but it is positioned far from the latter in the endocranial topology.

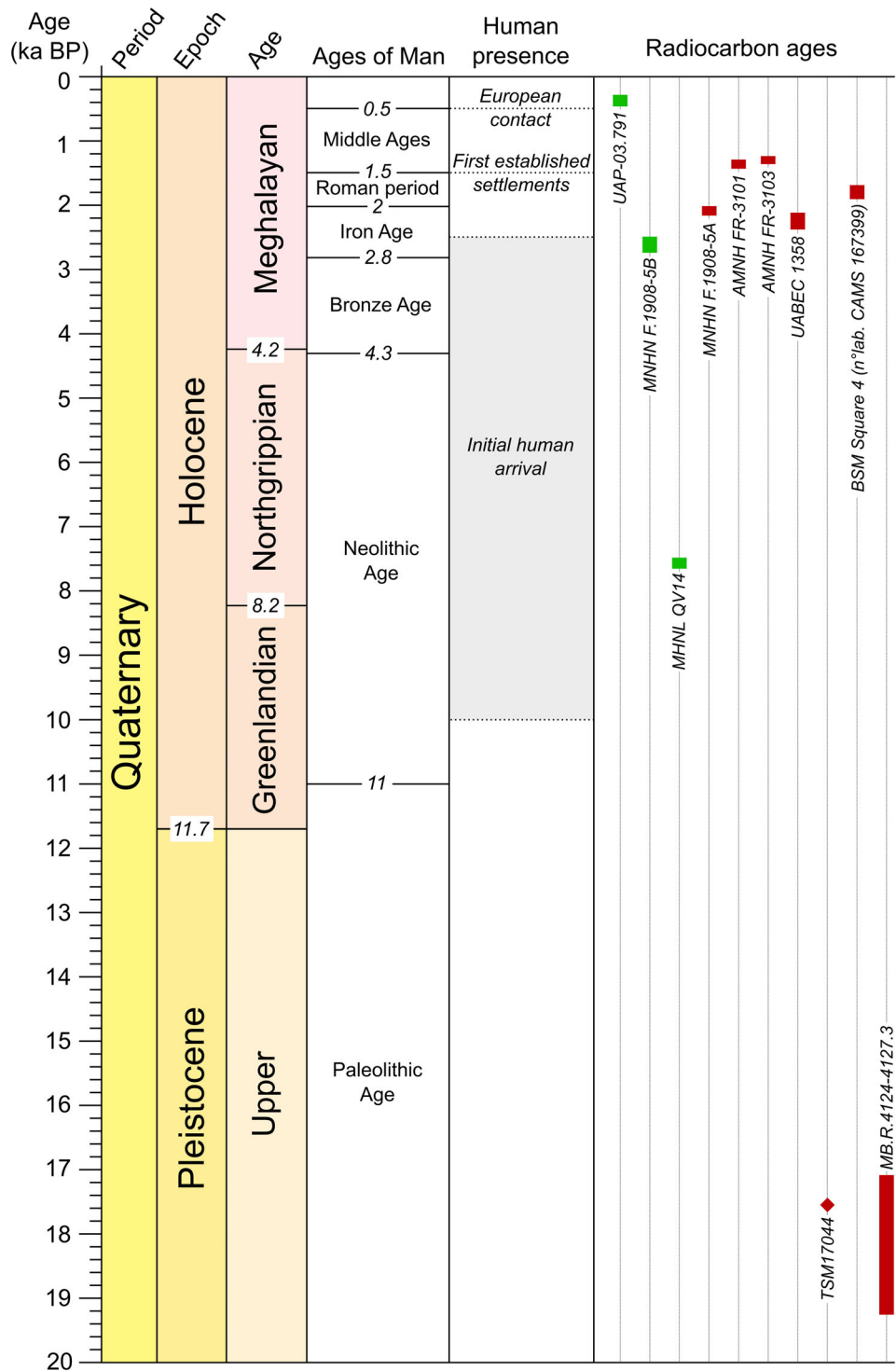
Such clustering of taxa controlled by rostrum shape, and particularly clustering of longirostrine forms, is a long standing problem in crocodylian phylogeny, which underlines many debates on cranial convergence and plasticity (Groh et al., 2019; Rio & Mannion, 2021). Here we observe that at first sight, part of our endocranial character matrix tends to produce the same results that external morphology struggle with. This trend seems linked to the nature of the characters chosen for this first analysis. Several character states referring to the shape of the paratympanic recesses, such as “bulbous” or “thin” are actually defining the volume of the cavities. Yet, a general compression of sinus diverticula occurs in meso-rostrine and longirostrine species (Perrichon, Hautier et al., 2023), changing the volume of recesses from “expanded” to “reduced,” in particular in the

basioccipital, pterygoid, basisphenoid, and median pharyngeal recesses. Compression of sinuses thus seems convergent with elongated skull shapes. Thus, as many characters involved in this first analysis account for the overall volume of air contained in the sinuses, which is greater in brevirostrine than in longirostrine species (Kuzmin et al., 2021; Perrichon, Hautier et al., 2023), such characters most likely reflect cranial convergences rather than true relationships. Moreover, character states defined as “expanded”/“bulbous,” or “reduced”/“thin” were found to be quite variable intraspecifically, showing that the expansion of several recesses is also dependent on the individual development of each specimen, and blurs the potential phylogenetic signal.

After pruning these irrelevant characters from the matrix, the second analysis recovered a topology seemingly more independent from cranial shape (Figure 18b). The position of several species in this tree can be discussed. First, *C. siamensis* and *C. palustris*, which are closely related species in molecular frameworks, are also clustered in our analysis. Their similar sinus morphology was already mentioned in Perrichon, Hautier et al. (2023) concerning the intertympanic diverticula, and may reflect their close relationships. However, the other relationships within the genus *Crocodylus* are either unresolved (i.e., *C. acutus*), or seem to reflect a convergence of sinus characters when considering molecular topologies. For instance, *C. halli* and *C. niloticus* are retrieved together based on sinus characters only, despite a large phylogenetic distance in molecular frameworks (Pan et al., 2021). The same phenomenon is observed with *C. porosus*, which is related to *C. siamensis* in most phylogenetic frameworks but is here positioned at the base of the genus according to sinus morphology (Figure 18b).

The position of *Mecistops* in the second topology echoes its position in the morphospace of pharyngotympanic sinus shape, where it is lying within *Crocodylus* species (Figure 15). Its pharyngotympanic sinus morphology and related discrete characters are for now unable to be robustly separated from *Crocodylus*. This is reminiscent of several morphological phylogenetic analyses, where *M. cataphractus* is retrieved as part of the *Crocodylus* clade, which originally led to its former denomination as “*Crocodylus*” *cataphractus* (Brochu, 1997, 2001, 2007; Rio & Mannion, 2021). In these topologies, *Mecistops* is generally positioned as a stem-branch of the genus *Crocodylus*. Thus, we show that its pharyngotympanic sinus and brain endocast morphology, like its cranial characters, are highly convergent with that of *Crocodylus*. However, *Mecistops* can still be distinguished from *Crocodylus* using intertympanic sinus morphology, as shown in Perrichon, Hautier, et al. (2023), when looking at the shape of the parietal recess and the relative growth of the

FIGURE 20 Compilation of known radiocarbon dates measured in Malagasy crocodylids found in the Late Quaternary of Madagascar. *Crocodylus* in green, *Voay robustus* in red. The stratigraphic table from the Holocene was adapted from Cohen et al. (2013); Georgopoulou et al. (2015). Information on human presence in Madagascar are compiled from Crowley (2010); Hansford et al. (2018); Douglass et al. (2019). Radiocarbon ages come from this study and from dated specimens of the literature listed in Data S1 and in Martin et al., 2022.



pneumatic preparietal processes. Despite this difference, the coding of these characteristics revealed to be difficult, and we failed to translate these features in suitable discrete characters in the current study. For now, only DNA sequencing seems able to decipher the phenotypic convergence involving this peculiar longirostrine genus.

Finally, in this analysis, *V. robustus* does not cluster with *Osteolaemus*, neither is it recovered as part of the

genus *Crocodylus*. This intermediate position reminds the results of Hekkala et al. (2021) using mitochondrial DNA, where *Voay* was recovered more related to *Crocodylus* than to *Osteolaemus*. Yet, we found that this position in our topology is only dependent on the coding of character 5, namely the presence of a rostral recess. However, the coding of the rostral recess in *Voay* is uncertain, as this structure is present in half of the specimens

studied and was thus coded as polymorphic (whereas its presence or absence is stable in all other studied species). Removing this character from the matrix leads to the collapse of this node, resulting in a polytomy between *Osteolaemus*, *Voay* and *Crocodylus* (Figure S16). Therefore, based on the studied endocranial characters, *Voay* can be excluded from the *Crocodylus* genus from an endocranial point of view, but its proximity with *Osteolaemus* cannot be assessed. This unresolved position is the same as what has been found by Brochu et al. (2022) using Bayesian inference on their full dataset of external morphological characters mixed with molecular data.

When adding our endocranial characters to a larger morphological character matrix, we find *Voay* clustered with *Osteolaemus* (Figure 19), which is consistent with other parsimony analyses using previous versions of this matrix (Brochu, 2007; Brochu et al., 2012, 2022; Brochu & Storrs, 2012). However, their shared sinus characters are not considered as synapomorphies in this topology, because they are also shared with *Alligator mississippiensis*. In this case, it confirms that the growth of the laterosphenoid, prootic and subcarotid recesses are convergent features linked to overall cranial shape. If *Voay* and *Osteolaemus* are indeed sister-taxa, the acquisition of such expanded sinus features by the two genera may have happened once in the branch leading to modern osteolaemines.

Looking on a larger scale, we find that the inclusion of endocranial characters has a major impact on the topology of Crocodylidae, especially on the relationships revolving around and inside the genus *Crocodylus*. First, the new topology implies a common sinus morphological change for *Crocodylus* and *Mecistops*, implying a single event of sinus reduction and resorption of sinus diverticula (Figure 19b). Then, the previously obtained polytomy of the genus (Figure 19a) now results in two main clades: one containing *C. niloticus* and Neotropical species, which has remained the same after adding endocranial characters; the other one grouping Indopacific species, with *C. siamensis* and *C. palustris* as sister-taxa. These results are particularly interesting for the phylogenetic hypotheses of Crocodylidae, because they are in line with recent molecular analyses (Hekkala et al., 2011; Milián-García et al., 2020; Pan et al., 2021), and also some recent morphological analyses focusing on the *Crocodylus* lineage (Delfino et al., 2020). Endocranial characters thus have a significant impact on morphological topologies, meaning that these features hold a non-negligible phylogenetic signal. In the future, investigating endocranial morphology for ontogenetic and intraspecific stability will be key to establish further valid characters that could resolve better these relationships and allow the expansion of the number of species included in such analyses.

8.3 | Palaeoecology of *V. robustus*

The similarities of endocranial morphology in *Voay* and *Osteolaemus* can be discussed to infer ecological information. In particular, the shape of their sinuses could be linked to ecological variables, making them useful to infer their behavior and living environment. The volumes of the sinuses have already been observed to shrink considerably in aquatic crocodylians such as thalattosuchians (Herrera et al., 2018; Wilberg et al., 2021), while it shows considerable inflation in fully terrestrial crocodylomorphs such as notosuchians (Pochat-Cottilloux et al., 2021, 2023). This trend could either be explained by directional selection on the buoyancy of the head, linked to the air-filled sinus cavities, or by developmental constraints of skull shape on sinus growth. *Osteolaemus* and *Voay* are nothing near notosuchian morphology, but their clearly enlarged sinuses compared to other extant crocodylians could reflect a less water-dependent lifestyle. Indeed, the African dwarf crocodile is unique, having the most “terrestrial” lifestyle among extant crocodylids. It is reported to live in swamps, periodically flooded forests, small pools or lakes, and is sometimes encountered far away from open water, taking walks to hunt small preys and making short journeys outside of water at night or after rain (Eaton, 2010; Kofron, 1992; Riley & Huchzermeyer, 1999; Shirley et al., 2017; Waitkuwait, 1986). *Voay* might have displayed a similar behavior, possibly living in swamps, wetlands and lakes rather than in open water compared to *C. niloticus*. This would have allowed the partition of the two species in different areas, and is also consistent with historical reports about habitat preferences of the putative remnants of *V. robustus* in the late 19th century (Vaillant & Grandidier, 1910). However, as mentioned by Bickelmann & Klein, 2009, it is highly unlikely that a crocodylian of the size and stature of *V. robustus*, similar to that of the Nile crocodile, would not be in competition with the latter, at least over food sources and territory. It is thus likely that *C. niloticus* could have participated to a certain extent in the decline of *Voay*, and ended up replacing it in most wet environments throughout the island.

8.4 | Biogeographical implications

The Malagasy crocodiles' faunal succession was originally thought to be sequential. First, *V. robustus* was considered extinct along other megafaunal species, following the arrival of humans or environmental changes on the island; then, *C. niloticus* supposedly colonized the island after *Voay* became extinct (Bickelmann & Klein, 2009; Brochu, 2007). This recent arrival was supported by a single radiocarbon dating at 360 ± 25 BP, and the presumed

absence of *C. niloticus* remains prior to this date (Crowley & Samonds, 2013). This has often led to numerous misidentifications of Malagasy crocodylian material found in Holocene deposits, wrongly attributed to *V. robustus*. However, molecular clock estimates of divergence timings between *C. niloticus* populations support a slightly older invasion around 2000–3000 BP (Hekkala et al., 2011), which could have implied a temporal overlap with *Voay*. Indeed, additional *Voay* specimens were dated in the past few years, which pushed forward their last occurrence datum at around 1300 BP (Figure 20; Godfrey et al., 2021; Hekkala et al., 2021; Samonds et al., 2019).

Known dated specimens of *Voay* now draws a minimal temporal range of existence spanning a period of roughly 18,000 years from the Upper Pleistocene to at least the first millennium A.C. (Figure 20). Regarding the temporal distribution of *C. niloticus*, two dated specimens now prove that *C. niloticus* did not arrive after the extinction of *Voay*, nor did it colonize the island recently in the Holocene (Martin et al., 2022). The age of the *Crocodylus* skull MNHN F.1908.5B, is here retrieved between 2750 and 2490 BP, which makes it roughly contemporaneous of the *Voay* specimens. The braincase MHNL QV14, attributed to a *Crocodylus* sp. and dated by Martin and colleagues (Martin et al., 2022) was retrieved at an even older age, around 7600 BP. These findings show that *C. niloticus* was indeed living on the island alongside *V. robustus* for at least two third of the Holocene (Figure 20). The modalities of the cohabitation between two large crocodiles in the same environment are still unknown without further knowledge on the ecology of *Voay*; but several avenues can be explored.

The localities where *Voay* fossil remains were found are situated in South-Western Madagascar and the Central Highlands, distributed from the coastline to the central plateau (Figure 2). The depositional palaeoenvironment of these localities corresponds to low-energy river systems and wetlands (i.e. flood plains, marshes and lakes) with one exception being a brackish interdunal swale (see Data S1 for details and reference on each locality). The *Voay* geographical distribution is thus slightly overlapping with that of the extant *Crocodylus*, the latter being also found in similar areas of the Central Highlands. The South West is nowadays mainly depleted of *Crocodylus* population, probably due to the large aridification of the area (Isberg et al., 2019).

The reports of Grandidier and Vaillant in their “*Histoire Naturelle des Reptiles [de Madagascar]*” about the Malagasy crocodile populations could potentially account for the latest encounters of living *V. robustus* specimens in the late 19th century (Vaillant & Grandidier, 1910). In these essays, based on local people accounts and in situ

observations, they described the morphology, distribution, and behavior of two crocodile morphotypes, namely “*Crocodylus madagascariensis*” (*Crocodylus niloticus*) and “*Crocodylus robustus*” (*V. robustus*). Vaillant and Grandidier (1910) stated that *C. niloticus* was then largely present throughout the island, particularly rivers and coastal settings in East and West Madagascar, whereas *V. robustus* was present only in a few lakes and marshes of the Central Highlands as well as in a few rivers and on the coast of the South-West, which agrees with the geographical position of fossil localities. The anatomical differences described, as well as drawings of the specimens, are however quite ambiguous and unconvincing, in the own word of the authors, which may indicate a confusion between large Nile crocodiles and *Voay*. However, the authors insisted on the systematic semantic separation in every Malagasy dialect between the two crocodile morphotypes, associated with a partition in geographical distribution and behavior. “*C.*” *robustus* is generally called “*Mamba*” and is of greater size and corpulence; it is described as dwelling in rather calm waters like lakes and marshes. *C.* “*madagascariensis*” is generally called “*Voay*” (the most used Malagasy word for “crocodile”) and is described as more “agile and gracile” and preferring rivers and coastlines. Still, one ethnic group (the Antifiherenanã), however, thought that *C. robustus* were only old *C. niloticus*, which adds to the uncertainty of this attribution. Whether or not this larger morphotype described by Grandidier really represents a remnant of a formerly larger *Voay* population, or a morphological variant of *C. niloticus* remains doubtful. In such cases, some pockets of *Voay* populations would have survived through the last millennium, and eventually showed a typical pattern of sheltering in small refuge areas of the Central highlands, before being slowly displaced by the invasive species from the mainland.

Four hypotheses can be made about the Malagasy crocodylians cohabitation and the extinction of *Voay*: (i) first, the two species had a similar ecology, filling the same ecological niche (proposed by Bickelmann & Klein, 2009), which would imply direct competition between the invasive and endemic species, and would have led to the extinction of *Voay*; (ii) second, the two species had different ecological preferences and filled two separate ecological niches, allowing for their cohabitation, the extinction of *Voay* would then be mainly due to habitat shrinking caused by human interactions and/or by the increased aridification of its living area in the Late Holocene (Burney, 1993, 2004; Crowley, 2010). (iii) third, *Voay* had a broader ecological range than *C. niloticus* and initially occupied most water ecosystems on the island, resulting in local competition and the displacement of *Voay* in refuge areas unfrequented by the invasive species, creating a partition of the two species on

the island before its extinction. (iv) *C. niloticus* had a broader ecological range than *Voay*, resulting in local competition in the only areas frequented by the endemic species, and its progressive displacement from its original living areas, leading to its extinction. Nevertheless, we do not yet know if the arrival of *Crocodylus* resulted from one or several colonization events, and we do not know either if the migration of *Crocodylus* originated solely from the African continent, because possibilities of transoceanic dispersal through the Indian Ocean cannot be excluded (Martin et al., 2022). These parameters remain unknown, and may complicate these scenarios.

In those cases, the extirpation of *Voay* from a part or whole of its living environment sped up its demise, as human implantation and increased aridity led to the drying of most marshes and wetlands in the South-West region. Only a few refuge areas would have been left in the highlands for the remnants of the endemic population to live in before its full extirpation. Alternatively, a combination of “passive” factors could have led to its decline: the aridification occurring in the South during the late Holocene could have been the primary trigger for the reduction of its living environment, leaving room for further implantation of *C. niloticus* in its place. Direct implication of humans cannot yet be confirmed; Bickelmann and Klein (2009) thought that the direct hunting of *Voay* would be unlikely, due to the stature of such a large reptile, but we know that very large animals such as *Aepyornis* have been hunted by the first humans on the island (Hansford et al., 2018), so this hypothesis cannot be discarded. However, Malagasy crocodiles had long been considered sacred by local people, generally preventing them to be killed for food or skin before the arrival of Europeans (Vaillant & Grandidier, 1910). Thus, the implication of humans would have been through their activities: egg hunting, implantation of settlements, and growing of livestock and agriculture may have considerably reduced the numbers and habitat of the endemic crocodile.

Finally, the prolonged cohabitation of *Crocodylus* and *Voay* and the overlapping of their living habitat could allow for a possible hybridization between the two species, especially in the context of their molecular phylogenetic relationships, as proposed by Hekkala et al. (2021). This extinction scenario tends to be less and less speculative considering the observed hybridization between extant *Crocodylus* species, which often occurs in distantly related species within the genus (Fitzsimmons et al., 2002). A mixing of genes between the two Malagasy populations could most likely have occurred, and could have participated in the decline of *Voay*, through the process of “genetic swamping” or “extinction by hybridization” (Hekkala et al., 2021; Rhymer & Simberloff, 1996).

Gathering of new specimens and further sequencing of ancient DNA in the future would certainly help in investigating such hypotheses.

9 | CONCLUSION

The internal anatomy of *Voay robustus* and especially, that of its paratympanic pneumaticity, are clearly different from *Crocodylus niloticus*. Several internal characters have been identified as autapomorphies, like the squared-shape pituitary fossa or the unpaired post-carotid pneumatic recess. Overall, the greater volume and the presence of additional recesses of the paratympanic sinuses in *Voay* recalls the morphology of *Osteolaemus*, with which it shares a close relationship based on external morphological evidence. Endocranial characters were tested and revealed to be prompt to convergence linked to cranial shape if not chosen properly. However, using them exclusively in a phylogenetic analysis failed to cluster *Voay* with *Osteolaemus* and rather echoes the molecular results, showing that even if its internal morphology is convergent with that of *Osteolaemus*, it may not be due to a close relationship. Although the clade Crocodylidae was better resolved overall, the addition of endocranial characters to an existing morphological matrix did not result in the recognition of new synapomorphies for Osteolaeminae. Sinus shape, in these two species, may be dependent on other variables, probably influenced by ecological or developmental constraints. Additionally, we hypothesize that the difference in sinus structures between *V. robustus* and *C. niloticus* could be linked to a slightly different lifestyle. We propose that *Voay* could have had behavioral habits like *Osteolaemus*, dwelling in swamps or lakes, despite occupying a larger part of these environments due to its greater size.

New radiocarbon dates of two specimens of *Voay* and *Crocodylus* from Madagascar, respectively dated to 2150 ± 22 and 2528 ± 22 BP, associated with other data from the literature, confirm the temporal overlap of *Crocodylus* and *Voay* throughout the Holocene. This implies some habitat partitioning in Madagascar upon the arrival of *Crocodylus*, perhaps favoured by behavioral differences. However, the greater adaptability of the invasive species, coupled with the habitat shrinking of *Voay* due to human implantation and/or the Late Holocene aridification would have sped up its extinction. Further examination of ancient DNA sequences would however be useful to assess if *Voay* and *Crocodylus* could have hybridized during the at least 8000 years of their cohabitation.

AUTHOR CONTRIBUTIONS

Gwendal Perrichon: Conceptualization; investigation; writing – original draft; methodology; visualization; writing – review and editing; formal analysis; data curation; resources; validation. **Yohan Pochat-Cottilloux:** Data curation; formal analysis; methodology; writing – review and editing. **Davide Conedera:** Investigation; data curation; formal analysis; writing – review and editing. **Pascale Richardin:** Formal analysis; resources; writing – review and editing; investigation. **Vincent Fernandez:** Resources; writing – review and editing; validation. **Lionel Hautier:** Methodology; validation; supervision; writing – review and editing. **Jeremy E. Martin:** Conceptualization; methodology; writing – review and editing; funding acquisition; supervision; project administration.

ACKNOWLEDGEMENTS

We thank Susannah Maidment (NHMUK), Ronan Allain (MNHN) and Nour-Edine Jalil (MNHN) who allowed the access, scanning and sampling of the fossil specimens. We address special thanks to Florent Goussard for the surface scanning of the MNHN specimens; Jeanne Rolland-Guillard, who helped with the initial stages of CT-scans segmentation; and Anh Nguyen Van, who prepared the samples for radiocarbon dating. We also thank Didier Berthet (MHNL), Salvador Bailon (MNHN), Emmanuel Robert and Blandine Bartschi (UCBL), Samuel Cordier (MZS), Anne-Lise Charruault (UM), Margarethe Maillart (SVSTUA), Bruno Vila (AMU), Christophe Borrelly (MHNM), and Patrick Campbell (NHMUK) for the access to the extant comparative specimens. Finally, we thank Heather Smith (Midwestern University), Jorgo Ristevski (University of Queensland, Australia), and Christopher Brochu (University of Iowa, United States), for insightful comments that improved the quality of this manuscript. This work was supported by the Agence Nationale de la Recherche (SEBEK project N° ANR19-CE31-0006-01 to JEM).

CONFLICT OF INTEREST STATEMENT

The authors declare that they have no competing interests.

DATA AVAILABILITY STATEMENT

Reconstructed volumes of *V. robustus* specimens and the three comparative specimens can be accessed on the online repository MorphoMuseum (Perrichon, Pochat-Cottilloux et al., 2023). CT data of other extant specimens used in the morphometric analyses will be published elsewhere and can eventually be obtained by asking the senior author. R scripts and character matrices are provided in the supplementary materials.

ORCID


Gwendal Perrichon  <https://orcid.org/0000-0001-5831-764X>

Yohan Pochat-Cottilloux  <https://orcid.org/0000-0002-6216-2721>

Pascale Richardin  <https://orcid.org/0000-0001-6741-0352>

Vincent Fernandez  <https://orcid.org/0000-0002-8315-1458>

Lionel Hautier  <https://orcid.org/0000-0001-8701-5421>

Jeremy E. Martin  <https://orcid.org/0000-0001-9159-645X>

REFERENCES

- Adams, D., Collyer, M., & Kaliontzopoulou, A. (2022). Geometric morphometric analyses of 2D/3D landmark data. *R Package Version 3.2*. <https://cran.ms.unimelb.edu.au/web/packages/geomorph/geomorph.pdf>
- Anderson, M. J. (2001). A new method for non-parametric multivariate analysis of variance: Non-parametric MANOVA for ecology. *Austral Ecology*, 26(1), 32–46. <https://doi.org/10.1111/j.1442-9993.2001.01070.pp.x>
- Angel, F. (1929). Sur une tête osseuse de Crocodile de Madagascar (*Crocodylus robustus* Grand. et Vaill.). *Bulletin du Museum National d'histoire Naturelle*, 1(3), 186–187.
- Barbour, T. (1918). Vertebrata from Madagascar: Amphibia and Reptilia. *Bulletin of the Museum of Comparative Zoology*, 16(14), 488.
- Beyrand, V., Voeten, D. F. A. E., Bureš, S., Fernandez, V., Janáček, J., Jirák, D., Rauhut, O., & Tafforeau, P. (2019). Multi-phase progenetic development shaped the brain of flying archosaurs. *Scientific Reports*, 9(1), 10807. <https://doi.org/10.1038/s41598-019-46959-2>
- Bickelmann, C., & Klein, N. (2009). The late Pleistocene horned crocodile *Voay robustus* (Grandidier & Vaillant, 1872) from Madagascar in the museum für Naturkunde Berlin. *Fossil Record*, 12(1), 13–21. <https://doi.org/10.1002/mmng.200800007>
- Brochu, C. A. (1997). Morphology, fossils, divergence timing, and the phylogenetic relationships of *Gavialis*. *Systematic Biology*, 46(3), 479–522.
- Brochu, C. A. (2001). Crocodylian snouts in space and time: Phylogenetic approaches toward adaptive radiation. *American Zoologist*, 41(3), 564–585.
- Brochu, C. A. (2003). Phylogenetic approaches toward Crocodylian history. *Annual Review of Earth and Planetary Sciences*, 31(1), 357–397. <https://doi.org/10.1146/annurev.earth.31.100901.141308>
- Brochu, C. A. (2007). Morphology, relationships, and biogeographical significance of an extinct horned crocodile (Crocodylia, Crocodylidae) from the quaternary of Madagascar. *Zoological Journal of the Linnean Society*, 150(4), 835–863. <https://doi.org/10.1111/j.1096-3642.2007.00315.x>
- Brochu, C. A. (2012). Phylogenetic relationships of Palaeogene ziphodont eusuchians and the status of *Pristichampsus* Gervais, 1853. *Earth and Environmental Science Transactions of the Royal Society of Edinburgh*, 103(3–4), 521–550. <https://doi.org/10.1017/S1755691013000200>
- Brochu, C. A., de Celis, A., Adams, A. J., Drumheller, S. K., Nestler, J. H., Benefit, B. R., Grossman, A., Kirera, F., Lehmann, T., Liutkus-Pierce, C., Manthi, F. K., McCrossin, M. L., McNulty, K. P., & Juma, R. N. (2022). Giant dwarf crocodiles from the Miocene of Kenya and crocodylid faunal dynamics in the late Cenozoic of East Africa. *The Anatomical Record*, 305, 1–37.

- Brochu, C. A., Parris, D. C., Grandstaff, B. S., Denton, R. K., & Gallagher, W. B. (2012). A new species of *Borealosuchus* (Crocodyliformes, Eusuchia) from the late cretaceous–early Paleogene of New Jersey. *Journal of Vertebrate Paleontology*, 32(1), 105–116. <https://doi.org/10.1080/02724634.2012.633585>
- Brochu, C. A., & Storrs, G. W. (2012). A giant crocodile from the Plio-Pleistocene of Kenya, the phylogenetic relationships of Neogene African crocodylines, and the antiquity of *Crocodylus* in Africa. *Journal of Vertebrate Paleontology*, 32(3), 587–602. <https://doi.org/10.1080/02724634.2012.652324>
- Bronzati, M., Benson, R. B. J., Evers, S. W., Ezcurra, M. D., Cabreira, S. F., Choiniere, J., Dollman, K. N., Paulina-Carabajal, A., Radermacher, V. J., Roberto-da-Silva, L., Sobral, G., Stocker, M. R., Witmer, L. M., Langer, M. C., & Nesbitt, S. J. (2021). Deep evolutionary diversification of semi-circular canals in archosaurs. *Current Biology*, 31(12), 2520–2529.e6. <https://doi.org/10.1016/j.cub.2021.03.086>
- Burney, D. (2004). A chronology for late prehistoric Madagascar. *Journal of Human Evolution*, 47(1–2), 25–63. <https://doi.org/10.1016/j.jhevol.2004.05.005>
- Burney, D. A. (1993). Late Holocene environmental changes in arid southwestern Madagascar. *Quaternary Research*, 40(1), 98–106. <https://doi.org/10.1006/qres.1993.1060>
- Cohen, K. M., Finney, S. C., Gibbard, P. L., & Fan, J.-X. (2013). The ICS international chronostratigraphic chart. *Episodes*, 36(3), 199–204. <https://doi.org/10.18814/epiugs/2013/v36i3/002>
- Colbert, E. H. (1946). The eustachian tubes in the Crocodylia. *Copeia*, 1946(1), 12. <https://doi.org/10.2307/1438813>
- Crowley, B. E. (2010). A refined chronology of prehistoric Madagascar and the demise of the megafauna. *Quaternary Science Reviews*, 29(19–20), 2591–2603. <https://doi.org/10.1016/j.quascirev.2010.06.030>
- Crowley, B. E., & Samonds, K. E. (2013). Stable carbon isotope values confirm a recent increase in grasslands in northwestern Madagascar. *The Holocene*, 23(7), 1066–1073. <https://doi.org/10.1177/0959683613484675>
- Cuvier (1807). Sur les différentes espèces de crocodiles vivants et sur leurs caractères distinctifs. *Annales du Muséum National d'Histoire Naturelle*, 10, 8–86.
- Delfino, M., Iurino, D. A., Mercurio, B., Piras, P., Rook, L., & Sardella, R. (2020). Old African fossils provide new evidence for the origin of the American crocodiles. *Scientific Reports*, 10(1), 11127. <https://doi.org/10.1038/s41598-020-68482-5>
- Douglass, K., Hixon, S., Wright, H. T., Godfrey, L. R., Crowley, B. E., Manjakahery, B., Rasolondrainy, T., Crossland, Z., & Radimilahy, C. (2019). A critical review of radiocarbon dates clarifies the human settlement of Madagascar. *Quaternary Science Reviews*, 221, 105878. <https://doi.org/10.1016/j.quascirev.2019.105878>
- Eaton, M. J. (2010). Dwarf Crocodile *Osteolaemus tetraspis*. In S.C. Manolis & C. Stevenson (Eds.), *Crocodyles* (3rd ed., pp. 127–132). Darwin: Crocodile Specialist Group.
- Fitzsimmons, N. N., Buchan, J. C., Lam, P. V., Polet, G., Hung, T. T., Thang, N. Q., & Gratten, J. (2002). Identification of purebred *Crocodylus siamensis* for reintroduction in Vietnam. *Journal of Experimental Zoology*, 294(4), 373–381. <https://doi.org/10.1002/jez.10201>
- George, I. D., & Holliday, C. M. (2013). Trigeminal nerve morphology in Alligator mississippiensis and its significance for crocodyliform facial sensation and evolution. *The Anatomical Record*, 296(4), 670–680. <https://doi.org/10.1002/ar.22666>
- Georgopoulou, E., Neubauer, T. A., Kroh, A., Harzhauser, M., & Mandic, O. (2015). An outline of the European quaternary localities with freshwater gastropods: Data on geography and updated stratigraphy. *Palaeontologia Electronica*, 18(3), 1–9. <https://doi.org/10.26879/527>
- Godfrey, L. R., Crowley, B. E., Muldoon, K. M., Burns, S. J., Scroxton, N., Klukkert, Z. S., Ranivoharimanana, L., Alumbaugh, J., Borths, M., Dart, R., Faina, P., Goodman, S. M., Gutierrez, I. J., Hansford, J. P., Hekkala, E. R., Kinsley, C. W., Lehman, P., Lewis, M. E., McGee, D., ... Widmann, P. (2021). Teasing apart impacts of human activity and regional drought on Madagascar's large vertebrate Fauna: Insights from new excavations at Tsimanampesotse and Antsirafaly. *Frontiers in Ecology and Evolution*, 9, 742203. <https://doi.org/10.3389/fevo.2021.742203>
- Goloboff, P. A., & Morales, M. E. (2023). TNT version 1.6, with a graphical interface for MacOS and Linux, including new routines in parallel. *Cladistics*, 39(2), 144–153. <https://doi.org/10.1111/cla.12524>
- Grandidier, A., & Vaillant, L. (1872). Sur le crocodile fossile d'Amboulintsatre (Madagascar). *Comptes Rendus Hebdomadaires des Seances de L'Academie des Sciences*, 75, 150–151.
- Groh, S. S., Upchurch, P., Barrett, P. M., & Day, J. J. (2019). The phylogenetic relationships of neosuchian crocodiles and their implications for the convergent evolution of the longirostrine condition. *Zoological Journal of the Linnean Society*, 188(2), 473–506. <https://doi.org/10.1093/zoolinnean/zlz117>
- Hansford, J., Wright, P. C., Rasoamiamanana, A., Pérez, V. R., Godfrey, L. R., Errickson, D., Thompson, T., & Turvey, S. T. (2018). Early Holocene human presence in Madagascar evidenced by exploitation of avian megafauna. *Science Advances*, 4(9), eaat6925. <https://doi.org/10.1126/sciadv.aat6925>
- Harshman, J., Huddleston, C. J., Bollback, J. P., Parsons, T. J., & Braun, M. J. (2003). True and false gharials: A nuclear gene phylogeny of Crocodylia. *Systematic Biology*, 52(3), 386–402. <https://doi.org/10.1080/10635150390197028>
- Hekkala, E., Gatesy, J., Narechania, A., Meredith, R., Russello, M., Aardema, M. L., Jensen, E., Montanari, S., Brochu, C., Norell, M., & Amato, G. (2021). Paleogenomics illuminates the evolutionary history of the extinct Holocene “horned” crocodile of Madagascar, *Voay robustus*. *Communications Biology*, 4(1), 1–11. <https://doi.org/10.1038/s42003-021-02017-0>
- Hekkala, E., Shirley, M. H., Amato, G., Austin, J. D., Charter, S., Thorbjarnarson, J., Vliet, K. A., Houck, M. L., Desalle, R., & Blum, M. J. (2011). An ancient icon reveals new mysteries: Mummy DNA resurrects a cryptic species within the Nile crocodile: Cryptic african *Crocodylus* species. *Molecular Ecology*, 20(20), 4199–4215. <https://doi.org/10.1111/j.1365-294X.2011.05245.x>
- Herrera, Y., Leardi, J. M., & Fernández, M. S. (2018). Braincase and endocranial anatomy of two thalattosuchian crocodylomorphs and their relevance in understanding their adaptations to the marine environment. *PeerJ*, 6, e5686. <https://doi.org/10.7717/peerj.5686>
- Hogg, A. G., Heaton, T. J., Hua, Q., Palmer, J. G., Turney, C. S., Southon, J., Bayliss, A., Blackwell, P. G., Boswijk, G., Ramsey, C. B., Pearson, C., Petchey, F., Reimer, P., Reimer, R., & Wacker, L. (2020). SHCal20 southern hemisphere calibration, 0–55,000 years cal BP. *Radiocarbon*, 62(4), 759–778. <https://doi.org/10.1017/RDC.2020.59>
- Hu, K., King, J. L., Romick, C. A., Dufeu, D. L., Witmer, L. M., Stubbs, T. L., Rayfield, E. J., & Benton, M. J. (2021). Ontogenetic endocranial shape change in alligators and ostriches and

- implications for the development of the non-avian dinosaur endocranium. *The Anatomical Record*, 304(8), 1759–1775. <https://doi.org/10.1002/ar.24579>
- Isberg, S., Combrink, X., Lippai, C., & Balaguera-Reina, S. A. (2019). *Crocodylus niloticus* (e.T45433088A3010181). The IUCN Red List of Threatened Species. <https://doi.org/10.2305/IUCN.UK.2019-1.RLTS.T45433088A3010181.en>
- Kazhdan, M., & Hoppe, H. (2013). Screened poisson surface reconstruction. *ACM Transactions on Graphics*, 32(3), 1–13. <https://doi.org/10.1145/2487228.2487237>
- Kofron, C. P. (1992). Status and habitats of the three African crocodiles in Liberia. *Journal of Tropical Ecology*, 8(3), 265–273. <https://doi.org/10.1017/S0266467400006490>
- Kuzmin, I. T. (2022). *anatomy, development and evolution of braincase in Crocodylomorpha (Diapsida: Archosauria)*. Saint Petersburg State University.
- Kuzmin, I. T., Boitsova, E. A., Gombolevskiy, V. A., Mazur, E. V., Morozov, S. P., Sennikov, A. G., Skutschas, P. P., & Sues, H.-D. (2021). Braincase anatomy of extant Crocodylia, with new insights into the development and evolution of the neurocranium in crocodylomorphs. *Journal of Anatomy*, 239(5), 983–1038. <https://doi.org/10.1111/joa.13490>
- Lessner, E. J., & Holliday, C. M. (2020). A 3D ontogenetic atlas of *Alligator mississippiensis* cranial nerves and their significance for comparative neurology of reptiles. *The Anatomical Record*, 305, ar.24550. <https://doi.org/10.1002/ar.24550>
- Martin, J. E., Richardin, P., Perrichon, G., Pochat-Cottilloux, Y., Phouybanhdyt, B., Salaviale, C., & Adrien, J. (2022). The oldest occurrence of *Crocodylus* in Madagascar and the Holocene crocodylian turnover. *Journal of Vertebrate Paleontology*, 41, e2063058. <https://doi.org/10.1080/02724634.2021.2063058>
- Meredith, R. W., Hekkala, E. R., Amato, G., & Gatesy, J. (2011). A phylogenetic hypothesis for *Crocodylus* (Crocodylia) based on mitochondrial DNA: Evidence for a trans-Atlantic voyage from Africa to the New World. *Molecular Phylogenetics and Evolution*, 60(1), 183–191. <https://doi.org/10.1016/j.ympev.2011.03.026>
- Milián-García, Y., Amato, G., Gatesy, J., Hekkala, E., Rossi, N., & Russello, M. (2020). Phylogenomics reveals novel relationships among neotropical crocodiles (*Crocodylus* spp.). *Molecular Phylogenetics and Evolution*, 152, 106924. <https://doi.org/10.1016/j.ympev.2020.106924>
- Mook, C. C., Matthew, W. D., & Wulsin, F. R. (1921). Description of a skull of the extinct Madagascar crocodile, *Crocodylus robustus* Vaillant and Grandidier. *Bulletin of the AMNH*, 44, 25–31. <https://digitallibrary.amnh.org/handle/2246/1727>
- Murray, C. M., Russo, P., Zorrilla, A., & McMahan, C. D. (2019). Divergent morphology among populations of the New Guinea crocodile, *Crocodylus novaeguineae* (Schmidt, 1928): Diagnosis of an independent lineage and description of a new species. *Copeia*, 107(3), 517. <https://doi.org/10.1643/CG-19-240>
- Oaks, J. R., & Dudley, R. (2011). A time-calibrated species tree of Crocodylia reveals a recent radiation of the true crocodiles. *Evolution*, 65(11), 3285–3297.
- Owen, R. (1842). Report on British fossil reptiles, part II. *Report for the British Association for the Advancement of Science, 1841*, 60–294.
- Pan, T., Miao, J.-S., Zhang, H.-B., Yan, P., Lee, P.-S., Jiang, X.-Y., Ouyang, J.-H., Deng, Y.-P., Zhang, B.-W., & Wu, X.-B. (2021). Near-complete phylogeny of extant Crocodylia (Reptilia) using mitogenome-based data. *Zoological Journal of the Linnean Society*, 191(4), 1075–1089. <https://doi.org/10.1093/zoolinlean/zlaa074>
- Perrichon, G., Hautier, L., Pochat-Cottilloux, Y., Raselli, I., Salaviale, C., Dailh, B., Rinder, N., Fernandez, V., Adrien, J., Lachambre, J., & Martin, J. E. (2023). Ontogenetic variability of the intertympanic sinus distinguishes lineages within Crocodylia. *Journal of Anatomy*, 242(6), 1096–1123. <https://doi.org/10.1111/joa.13830>
- Perrichon, G., Pochat-Cottilloux, Y., Conedera, D., Richardin, P., Fernandez, V., Hautier, L., & Martin, J. E. (2023). 3D models related to the publication: Neuroanatomy and pneumaticity of the extinct Malagasy “horned” crocodile *Voay robustus* and its implications for crocodylid phylogeny and palaeoecology. *MorphoMuseum*, e205. <https://doi.org/10.18563/journal.m3.205>
- Pochat-Cottilloux, Y., Martin, J. E., Jouve, S., Perrichon, G., Adrien, J., Salaviale, C., de Muizon, C., Cespedes, R., & Amiot, R. (2021). The neuroanatomy of *Zulmasuchus querejazus* (Crocodylomorpha, Sebecidae) and its implications for the paleoecology of sebecosuchians. *The Anatomical Record*, 305(10), 2708–2728. <https://doi.org/10.1002/ar.24826>
- Pochat-Cottilloux, Y., Rinder, N., Perrichon, G., Adrien, J., Amiot, R., Hua, S., & Martin, J. E. (2023). The neuroanatomy and pneumaticity of *Hamadasuchus* (Crocodylomorpha, Peirosauridae) from the cretaceous of Morocco and its paleoecological significance for altirostral forms. *Journal of Anatomy*, 00, 1–20. <https://doi.org/10.1111/joa.13887>
- Porter, W. R., Sedlmayr, J. C., & Witmer, L. M. (2016). Vascular patterns in the heads of crocodylians: Blood vessels and sites of thermal exchange. *Journal of Anatomy*, 229(6), 800–824. <https://doi.org/10.1111/joa.12539>
- R Core Team. (2021). *R: A language and environment for statistical computing*. R Foundation for Statistical Computing <https://www.R-project.org/>
- Rakotozandry, R., Ranivoharimanana, L., Ranaivosoa, V., Rasolofomanana, N., Hekkala, E., & Samonds, K. E. (2021). Description of the subfossil crocodylians from a new late Pleistocene subfossil site (Tsaramody, Sambaina Basin) in Central Madagascar. *Malagasy Nature*, 15, 94–107.
- Rhymer, J. M., & Simberloff, D. (1996). Extinction by hybridization and introgression. *Annual Review of Ecology and Systematics*, 27(1), 83–109. <https://doi.org/10.1146/annurev.ecolsys.27.1.83>
- Richardin, P., Porcier, S., Ikram, S., Louarn, G., & Berthet, D. (2017). Cats, crocodiles, cattle, and more: Initial steps toward establishing a chronology of ancient Egyptian animal mummies. *Radiocarbon*, 59(2), 595–607. <https://doi.org/10.1017/RDC.2016.102>
- Riley, J., & Huchzermeyer, F. W. (1999). African dwarf crocodiles in the Likouala swamp forests of The Congo Basin: Habitat, density, and nesting. *Copeia*, 1999(2), 313–320. <https://doi.org/10.2307/1447477>
- Rio, J. P., & Mannion, P. D. (2021). Phylogenetic analysis of a new morphological dataset elucidates the evolutionary history of Crocodylia and resolves the long-standing gharial problem. *PeerJ*, 9, e12094. <https://doi.org/10.7717/peerj.12094>
- Samonds, K. E., Crowley, B. E., Rasolofomanana, T. R. N., Andriambelomanana, M. C., Andrianavalona, H. T., Ramihan gihajason, T. N., Rakotozandry, R., Nomenjanahary, Z. B., Irwin, M. T., Wells, N. A., & Godfrey, L. R. (2019). A new late Pleistocene subfossil site (Tsaramody, Sambaina basin, Central Madagascar) with implications for the chronology of habitat and

- megafaunal community change on Madagascar's central highlands. *Journal of Quaternary Science*, 34(6), 379–392. <https://doi.org/10.1002/jqs.3096>
- Schneider, C. A., Rasband, W. S., & Eliceiri, K. W. (2012). NIH image to ImageJ: 25 years of image analysis. *Nature Methods*, 9(7), 671–675. <https://doi.org/10.1038/nmeth.2089>
- Shirley, M. H., Burtner, B., Oslisly, R., Sebag, D., & Testa, O. (2017). Diet and body condition of cave-dwelling dwarf crocodiles (*Osteolaemus tetraspis*, cope 1861) in Gabon. *African Journal of Ecology*, 55(4), 411–422. <https://doi.org/10.1111/aje.12365>
- Tahara, R., & Larsson, H. C. E. (2022). Paratympenic sinuses in juvenile alligator. *The Anatomical Record*, 305(10), 2926–2979. <https://doi.org/10.1002/ar.24932>
- Vaillant, L., & Grandidier, G. (1910). *Histoire physique, naturelle, et politique de Madagascar. Volume XVII, Histoire naturelle des reptiles; première partie: crocodiles et tortues*. AbeBooks.
- Waitkuwait, W. E. (1986). *Present knowledge on the west African slender-snouted crocodile, Crocodylus cataphractus Cuvier 1824 and the west African dwarf crocodile Osteolaemus tetraspis cope 1861, Crocodiles. Their ecology, management, and conservation* (pp. 260–275). IUCN.
- Walsh, S. A., Barrett, P. M., Milner, A. C., Manley, G., & Witmer, L. M. (2009). Inner ear anatomy is a proxy for deducing auditory capability and behaviour in reptiles and birds. *Proceedings of the Royal Society B: Biological Sciences*, 276(1660), 1355–1360. <https://doi.org/10.1098/rspb.2008.1390>
- Watanabe, A., Gignac, P. M., Balanoff, A. M., Green, T. L., Kley, N. J., & Norell, M. A. (2019). Are endocasts good proxies for brain size and shape in archosaurs throughout ontogeny? *Journal of Anatomy*, 234(3), 291–305. <https://doi.org/10.1111/joa.12918>
- White, E. I. (1930). *Fossil hunting in Madagascar*. Trustees of the British Museum.
- Wickham, H. (2011). ggplot2, *WIREs. Computational Statistics*, 3(2), 180–185. <https://doi.org/10.1002/wics.147>
- Wilberg, E. W., Beyl, A. R., Pierce, S. E., & Turner, A. H. (2021). Cranial and endocranial anatomy of a three-dimensionally preserved teleosauroid thalattosuchian skull. *The Anatomical Record*, 305, 2620–2653. <https://doi.org/10.1002/ar.24704>

SUPPORTING INFORMATION

Additional supporting information can be found online in the Supporting Information section at the end of this article.

How to cite this article: Perrichon, G., Pochat-Cottilloux, Y., Conedera, D., Richardin, P., Fernandez, V., Hautier, L., & Martin, J. E. (2023). Neuroanatomy and pneumaticity of the extinct Malagasy “horned” crocodile *Voay robustus* and its implications for crocodylid phylogeny and palaeoecology. *The Anatomical Record*, 1–38. <https://doi.org/10.1002/ar.25367>